NTNU – Trondheim
Norwegian University of
Science and Technology

Modelling and Control of Thruster Assisted Position Mooring System for a Semi-submersible

Analysis and Model Testing

Solveig Bjørneset

Marine Technology
Submission date: June 2014
Supervisor: Asgeir Johan Sørensen, IMT
Co-supervisor: Anne Marthine Rustad, IMT
Ivar Ihle, Rolls Royce

Norwegian University of Science and Technology
Department of Marine Technology

NTNU Trondheim
Norwegian University of Science and Technology
Department of Marine Technology

MASTER THESIS IN MARINE CYBERNETICS

SPRING 2014

FOR

STUD. TECH. Solveig Bjørneset

Modelling and Control of Thruster Assisted Position Mooring System for a Rig

Analysis and Model Testing

Work description

The main objective of this Master Thesis is to study the interaction between a thruster assisted rig and its passive mooring system, especially the yaw dynamics. Fuel reduction, wider operational window, and redundancy are some of the reasons why thruster assisted position mooring systems are widely used.

Slow resonant motions will be reduced, and stability and robustness will be obtained for the total system. The control objectives will include reducing coupled motions, ensuring station keeping for a large operation window, and fault monitoring and control. The objectives are achieved through introduction of a roll and pitch damping controller, general motion reduction by a nonlinear passive control law, and a set-point chasing algorithm. Testing will be conducted through simulations in Matlab Simulink and through model tests in two test series during the spring of 2014. The results will be presented in a closing Master Thesis.

Scope of work

- Review relevant literature on thruster assisted position mooring.
- Define requirements for the POSMOOR system including metocean data, water depth and mooring spread for operation in the North Sea. Define scaled requirements for the model test.
- Conduct simulations with controller and study the total system dynamics for varying environmental conditions through simulation.
- Plan and prepare model scale experiments for CyberRig I. Decide test plan including which control methods, controller objectives, and environmental conditions to be tested.
- Conduct two model test series, in weeks 12 and 20. Test of total control system performance will be conducted, using controller and environmental parameters evaluated during the previous steps.
- Compare simulation result and model test results. Use conclusions drawn from the first model tests to plan and prepare the second model test series.
- Document each step in the process.

The report shall be written in English and edited as a research report including literature survey, description of mathematical models, description of control algorithms, simulation results, model test results, discussion and a conclusion including a proposal for further work. Source code should be provided on a CD with code listing enclosed in appendix. It is supposed that Department of Marine Technology, NTNU, can use the results freely in its research work, unless otherwise agreed upon, by referring to the student's work. The thesis should be submitted in three copies within June 10th.

Advisers: Associated prof. II Anne Marthine Rustad and Dr. Ivar Ihle, Rolls Royce

Professor Asgeir J. Sørensen
Supervisor

Preface

This Master's Thesis has been written during the spring of 2014 as the concluding part of a Master of Science degree in Marine Cybernetics at NTNU. Different solutions for control methods in position mooring has been studied, especially the roll and pitch damping control law. A theoretical stability analysis has been derived, a simulation model of the system has been developed and physical model tests have been carried out, testing the performance of combined nonlinear passive observer, nonlinear PID, and a roll and pitch damping control law.

First of all, I would like to thank my supervisor Professor Asgeir Sørensen for the inspiration and good advices I have received. I would also like to thank my advisors Professor II Anne Marthine Rustad and Dr. Ivar-André F. Ihle for steady and determined guidance through the process of writing this Master's Thesis.

The mathematical mooring cable model, created by Prof. Ole Morten Aamo and Prof. Thor Inge Fossen, was provided to me by Dr. Per Ivar Barth Berntsen, for which I am thankful. The model is used with consent from Aamo and Fossen, and has solved a lot of challenges regarding the simulation model.

Thanks to Stefano Bertelli for assistance with the modelling of CyberRig I, for giving me practical insight in model testing, and for providing several power supplies for CyberRig I. The lab supervisor Torgeir Wahl has been able to answer all my questions and help me out with the outdated software and control set-up of CyberRig I, even when the model semi-submersible started taking on water. Funding for repair of the model was provided by the Department of Marine Technology.

Solveig Bjørneset
June 17, 2014, Trondheim

Abstract

In recent years, thruster assisted position mooring systems have become more commersially available, especially in the oil industries. The vessels tend to operate in harsh weather more frequently, and the desire for a larger weather window is inevitably present.

For harsh weather, nonlinear effects dominate the dynamics to a larger extent than for calm weather. The low frequency dynamics of a moored vessel are excited by second order wave drift forces. To counteract the low-frequency resonant dynamics of the mooring system, proper control methods are derived and carefully applied. For this purpose, several control laws have been selected and studied.

The control objectives are reduction of fuel consumption, increased redundancy, and higher stationkeeping precision for harsh weather. The control methods studied include reduction of coupled dynamics by implementation of a roll and pitch damping controller, optimal setpoint chasing based on a structural reliability criteron, and a backstepping control law based on the same reliability criterion. These three methods, combined with a nonlinear passive observer, have been studied and found both stable and robust. Especially, a theoretical six degrees of freedom Lyapunov stability analysis is performed, which renders the combined PID, and roll and pitch damping controller globally asymptotically stable. Stability properties for all considered control methods have been clarified.

A simulation model for testing of the different control methods is derived and implemented in Matlab Simulink. The simulation model is based on a typical full scale semi-submersible anchored with mooring cables in a circular anchor configuration. A nonlinear passive observer is implemented and tuned to give satisfactory estimates for all six degrees of freedom.

Model tests are performed in the Marine Cybernetics Laboratory at NTNU using the 1:100 model semi-submersible CyberRig I. Model tests are performed for regular and irregular waves, with and without thruster force input. The process of obtaining sufficient closed-loop wave-filtered roll and pitch angular velocity estimates in model scale has proved challenging.

Sammendrag

I de senere årene har thrusterassisterte oppankringssystemer blitt mer kommersielt tilgjengelige, spesielt i oljeindustrien. Fartøyene har en tendens til å operere i tøffere værforhold oftere, og trangen for et større værvindu er uunngåelig tilstede.

For tøffe værforhold vil ikke-lineære effekter dominere dynamikken i større grad enn for rolig vær. Den lavfrekvente dynamikken til det forankrede fartøyet blir eksitert av andreordens bølgedriftkrefter. For å dempe den lavfrekvente resonante dynamikken i forankringssystemet, må riktige kontrollmetoder utledes og anvendes omhyggelig. Flere kontrollere har blitt utvalgt og studert for dette formålet.

Målsetningene for kontrollalgoritmene er reduksjon av drivstoffforbruket, økt redundans og høyere stasjonær presisjon. Metodene studert i denne masteroppgaven omfatter reduksjon av koblede bevegelser ved implementasjon av en dempekontroller i rull og stamp, optimalt settpunktjag basert på et strukturelt pålitelighetskriterium, og en tilbakekoblet kontrollov basert på det samme pålitelighetskriteriet. Disse tre metodene, sammen med en ikke-lineær passiv observatør, har blitt studert og funnet å være både stabile og robuste. Verd å trekke frem er en teoretisk Lyapunov stabilitetsanalyse i seks frihetsgrader for rull- og stampdemperen kombinert med en PID-regulator. Analysen gir global asymptotisk stabilitet for den kombinerte kontrolloven. Det er gjort rede for stabilitetsegenskapene til alle de nevnte kontrollmetodene.

En simuleringsmodell for testing av kontrollmetodene er utviklet og implementert i Matlab Simulink. Simuleringsmodellen er basert på en typisk fullskala halvt nedsenkbar plattform oppankret med en sirkulær ankerkonfigurasjon. En ulineær passiv obervatør er implementert og finstemt til å gi tilfredsstillende estimater i alle de seks frihetsgradene.

Modelltester er utført i MC-Laben på NTNU ved bruk av den 1:100 modellplattformen CyberRig I. Modellen er testet i regulære og irregulære bølger, både med og uten thrusterpådrag. Prosessen med å fremskaffe tilstrekkelige estimater for bølgefiltrerte vinkelhastigheter i rull og stamp i lukket sløyfe i modellskala har vist seg å være utfordrende.

Table of Contents

Nomenclature

Abbreviations

CB	**C**enter of **B**uoyancy
CDF	**C**umulative **D**istribution **F**unction
CG	**C**enter of **G**ravity
CPM	**C**ontrol **P**lant **M**odel
DOF	**D**egrees **O**f **F**reedom
DP	**D**ynamic **P**ositioning
GAS	**G**lobal **A**symptotical **S**tability
GES	**G**lobal **E**xponential **S**tability
HF	**H**igh-**F**requency
HMI	**H**uman-**M**achine **I**nterface
ISS	**I**nput to **S**tate **S**table
KF	**K**alman **F**iltering
KYP	**K**alman **Y**akubovich **P**opov (lemma)
LFC	**L**yapuov **F**unction **C**andidate
LF	**L**ow-**F**requency
MCLab	**M**arine **C**ybernetics **Lab**oratory
ML	**M**ooring **L**ine
NED	**N**orth-**E**ast-**D**own
NPO	**N**onlinear **P**assive **O**bserver
PDE	**P**artial **D**ifferential **E**quations
PID	**P**roportional-**I**ntegral-**D**erivative
PM	**P**osition **M**ooring
PPM	**P**rocess **P**lant **M**odel
RAO	**R**esponse **A**mplitude **O**perator
RPD	**R**oll and **P**itch **D**amping
SPR	**S**trictly and **P**ositive **R**eal

WF **W**ave-**F**requency

Greek Letters

α_i	Horizontal angle of mooring force for mooringline number *i*
$\boldsymbol{\eta}$	Position vector of vessel
$\boldsymbol{\eta}_0$	Moored resting position vector of vessel
$\boldsymbol{\eta}_h$	Horizontal longitudinal position vector of vessel
$\boldsymbol{\nu}$	Velocity vector of vessel
$\boldsymbol{\nu}_c$	Current velocity vector
$\boldsymbol{\nu}_h$	Horizontal longitudinal velocity vector of vessel
$\boldsymbol{\nu}_r$	Relative velocity vector of vessel
$\boldsymbol{\omega}$	Angular velocities of vessel
$\boldsymbol{\tau}_{hyd}$	Hydrodynamic forces and moments
$\boldsymbol{\tau}_{moor}$	Mooring system forces and moments
$\boldsymbol{\tau}_{RB}$	Generalized vector of external forces
$\boldsymbol{\tau}_{wave1}$	Linear wave forces
$\boldsymbol{\tau}_{wave2}$	Second-order wave forces
$\boldsymbol{\tau}_{wave}$	Wave forces
$\boldsymbol{\tau}_{wind}$	Wave forces
$\boldsymbol{\Theta}$	Attitude (Euler angles) of vessel
$\boldsymbol{\xi}$	Wave frequency motion vector
$\Delta\omega$	Incremental step in wave spectrum integration
ϵ	Phase angle of wave
γ_{rw}	Wind angle of attack
λ	Scaling parameter
∇	Vessel displacement
ω	Oscillation frequency of wave
ω	Rotational speed of propeller
ϕ	Roll angle of vessel
ψ	Yaw angle of vessel
ρ	Density of water
ρ_0	Mass per unstretched unit length of cable
ρ_a	Mass density of air
ρ_w	Density of sea water
τ	Forces acting on the vessel
θ	Pitch angle of vessel
θ_m	Fixed thruster parameters
ξ_m	Variable thruster parameters

ζ	Wave amplitude

Roman Letters

A	Wave amplitude
a_F	Acceleration of full scale vessel
A_{Fw}	Wind projected area in surge
A_{Lw}	Wind projected area in sway
A_{wp}	Vessel area in the water plane
A_w	Wave filtering system matrix
$\mathbf{C}_A$	Hydrodynamic coriolis and centripetal matrix
$\mathbf{C}_{RB}$	Rigid body coriolis and centripetal matrix
C_w	Wave filtering measurement matrix
$C_{X,\ldots,N}$	Wind force coefficients
$\mathbf{D}_L$	Linearized hydrodynamic damping matrix
$\mathbf{D}_{mo}$	Linearized damping term of mooring system
$\mathbf{d}_{mo}$	Damping term of mooring system
$\mathbf{D}_{NL}$	Nonlinear hydrodynamic damping matrix
e	Cable strain
E_w	Wave filtering disturbance matrix
$\mathbf{f}$	External forces working on cable
$\mathbf{f}_{(dn)}$	Normal drag forces working on cable
$\mathbf{f}_{(dt)}$	Tangential drag forces working on cable
$\mathbf{f}_{(hg)}$	Gravity and hydrostatic forces working on cable
$\mathbf{f}_{(mn)}$	Hydrodynamic added inertia forces working on cable
$\overline{GM}_L$	Longitudinal metacentric height
$\overline{GM}_T$	Transverse metacentric height
$\mathbf{G}$	Hydrostatic restoring matrix
$\mathbf{G}_{mo}$	Linearized stiffness of mooring system
$\mathbf{g}_{mo}$	Stiffness of mooring system
g	Gravitational acceleration
h	Depth of mooring system
H_s	Significant wave height
H_{Fw}	Centroid of wind projected area in surge
H_{Lw}	Centroid of wind projected area in sway
$\mathbf{I}$	Identity matrix
$\mathbf{I}_s$	Rotational inertia of propeller
K_ϕ	Restoring in roll due to roll motion
$\mathbf{M}_A$	Added mass matrix
$\mathbf{M}_{RB}$	Rigid body mass matrix

M_θ	Restoring in pitch due to pitch motion
n	Rotational speed of propeller
o_b	Origin of body-fixed reference frame
o_n	Origin of NED-frame
$\mathbf{p}$	Translational position of vessel
$\mathbf{p}_h$	Horizontal position of vessel
p	Angular velocity of vessel in roll
P_a	Propeller power
q	Angular velocity of vessel in pitch
Q_a	Propeller load torque
Q_c	Commanded motor torque
Q_f	Shaft friction
Q_m	Motor torque
$\mathbf{r}$	Cable position vector
$\mathbf{r}_g$	Distance from origin to center of gravity
r	Angular velocity of vessel in yaw
S	Wave spectrum
$S(\cdot)$	Cross product operator
T	Cable tension
t	Time variable
T_0	Peak wave period
T_1	Average wave period
T_a	Propeller thrust
T_i	Horizontal mooring force for MLi
T_z	Average zero-crossing period
T_{kk}^{ic}	Second order wave force coefficient
u	Longitudinal velocity of vessel in surge
u_c	Current velocity in surge direction
$\mathbf{v}$	Translational velocity vector of vessel
$\mathbf{v}$	Velocity of cable
$\mathbf{v}_h$	Horizontal velocity vector of vessel
v	Longitudinal velocity of vessel in sway
v_c	Current velocity in sway direction
V_{rw}	Absolute relative wind speed
$\mathbf{w}$	Trial function used in discretization
w	Longitudinal velocity of vessel in heave
$\bar{x}_i$	Longitudinal position of spread mooring point i
x	Longitudinal position of vessel in surge
$\bar{y}_i$	Longitudinal position of spread mooring point i

y	Longitudinal position of vessel in sway
z	Longitudinal position of vessel in heave
Z_z	Restoring in heave due to heave motion

Chapter 1

Introduction

In recent years, thruster assisted position mooring systems have become more commersially available, especially in the oil industry, according to Sørensen (2011). Both turret moored systems and spread moored systems are widely used. For semi-submersibles, it is suitable to use spread moored systems.

Lately there have been reported a number of cases where excessive roll and pitch motions have caused operational difficulties for semi-submersibles. Because of the semi-submersible's shape, with small-waterplane-area columns and relatively small pontoons, the inertia, damping and restoring forces in roll and pitch are small in comparison with other constructions of equal mass. It should be mentioned that excessive motions in heave due to first order loads in rough seas is yet another reason for concern. This issue will not be mentioned further.

The excessive roll and pitch motions are found to be resulting from both linear and nonlinear effects, that is, both wave-frequency and low-frequency effects. Counteracting the wave-frequency roll and pitch motions by thruster force is quite useless. It is the low-frequency motions that should be damped, which means that sufficient low-pass filtered roll and pitch rotational velocity estimates need to be obtained. This places great demands on the performance of the observer.

In order to reduce slow resonant motions and obtain stability in thruster assisted position mooring, several control laws have been proposed and studied. The control objectives are reduction of fuel cost, increased redundancy, and higher station keeping precision. The methods studied in this Master's Thesis include reduction of coupled motions by implementation of a roll and pitch damping controller, optimal setpoint chasing based on a structural reliability criteron, and a backstepping control law based on the same reliability criterion. These three methods along with a nonlinear passive observer have been studied and proven to be both stable and robust.

1.1 Previous Scientific Work

To fully understand the current status of position mooring today, some of the theoretical development from the early start till today is reviewed.

1.1.1 Mooring

In the offshore industry, the first attempt at coring using a moored ship was conducted offshore California in 1953 at 120 [m] depth, Faÿ (1990). Prior to this, coring had only been performed from fixed structures. One year later, the first floating vessel was used for drilling in the Gulf of Mexico.

Unfortunately, when going for deeper waters, the passive mooring system has got too much horizontal elasticity and too little hydrodynamic damping to keep the vessel in a position steady enough to perform safe drilling operations. The cost and the complexity of the mooring system are also increasing with depth. These drawbacks contributed to the development of the dynamic positioning system.

1.1.2 Dynamic Positioning

Phase one of the Mohole Project was conducted in 1961, where the vessel CUSS 1 held position within a circle of radius 180 [m] by manual control of thrusters, as narrated in Faÿ (1990). Later that year, another vessel called Eureka was equipped with the first computer based positioning system. After this, there has been a steady evolution of dynamic positioning systems. Among the highlights are the invention of Kalman Filtering and the dive into optimal control theory.

In the 1990's, an approach towards even smarter design methods for dynamic positioning systems started. This development was pushed forward by the desire for a control system which could take system dynamics and limitations into account. One method, which several functions have been built upon later, is model-based design. A model-based control system design was presented in Sørensen, Sagatun, and Fossen (1996).

The model-based passive nonlinear observer was introduced in Fossen and Strand (1999). The nonlinear passive observer yields global exponential stability (GES), while the linear Kalman Filter (KF) theory does not.

A roll and pitch damping (RPD) controller was introduced in Strand and Sørensen (2000), and proved to damp horizontal motions by exploiting the hydrodynamic couplings between surge and pitch, and sway and roll degrees of freedom.

The theory of hybrid control was first implemented in air- and land-based vehicles. During the course of previous years, hybrid control has also been applied in dynamic positioning.

The need for stability in the total control system, including the switching logic, places special requirements on the control system design. Hybrid control is discussed in, among others, Teel, Sanfelice, and Goebel (2011), Nguyen (2006), and Nguyen and Sørensen (2009b).

1.1.3 Position Mooring

Mooring the vessel is a low cost solution, offering stationkeeping steady enough for most operations performed in shallow water and calm weather conditions. Dynamic positioning, on the other hand, is a high-cost solution compared to passive mooring only. The third option is a merge between mooring and dynamic positioning, called thruster assisted mooring or position mooring (PM). For PM systems, the passive mooring system provides most of the horizontal damping. The thrusters must assist the passive mooring system for environmental or operational conditions which challenge the properties of the passive mooring system.

The first published combination of thruster assistance and mooring was presented in Strand, Sørensen, and Fossen (1998). Position keeping based on adjusting the mooring line lengths using winches was proposed by Aamo and Fossen (1999). Adjusting the mooring line lengths impose large and oscillating forces on the winches, causing wear and tear, even if only the LF motions are to be counteracted. The theory of implementing this control method is therefore not used in the industry.

Imposing a structural reliability criterion on riser angles was done in Leira, Sørensen, and Larsen (2002). In Fang et al. (2013), setpoint chasing based on mooring line tension was performed. The task of reaching the desired setpoint is handled by a control law, e.g. PID. A nonlinear feedback control law based on the same structural reliability criterion was derived by Berntsen, Aamo, and Leira (2006) using backstepping techniques. The structural reliability criterion was originally used in the field of construction. The implementation of one of the mentioned algorithms could minimize the risk of mooring line failure to a large extent. Position mooring was first merged with hybrid control in Nguyen and Sørensen (2009a). Hybrid control is believed to be tomorrow's solution for both DP and PM.

1.1.4 Official Standards

In terms of rules and legislation, position mooring has been regulated for several years. The *DNV Offshore Standards on Position Mooring*, DNV (2013), is updated on a regular basis. As of today, mooring systems are designed to handle the loss of one anchor line out of twelve. A requirement for the system being able to handle the loss of two mooring lines is being dicussed (autumn 2013) and added as an optional requirement. If the mentioned

requirement should become effective, a robust and fault detecting position mooring system might become required for high-risk operations.

1.2 Motivation

The main objective of this Master's Thesis is to study the interaction between a thruster assisted mooring system and its passive mooring system. The main goal is increased stability for all degrees of freedom for harsh weather. Some of the other objectives that can be achieved through a successfull merge between mooring and thruster assistance, are:

- Reducing fuel consumption compared to regular DP systems (no mooring)
- Increasing positioning accuracy compared to passive mooring only
- Decreasing the possibility of mooring line breakage
- Ensuring mooring line integrity
- Larger operational window
- Increasing dynamic stability

An algorithm that manages to combine the dynamics of both the mooring system and the thrust allocation system in a good manner, is the key to a stable and robust thruster assisted position mooring system.

Position mooring for a rig operating in the North Sea is studied. There are several possibilities for control system improvement related to position mooring. The North Sea is a harsh environment where storms and bad weather often lead to downtime for offshore operations. Position mooring system might decrease downtime by expanding the weather window for several conditions.

Position mooring is able to make traditional mooring safer, by using safety criteria which account for loss of mooring lines, anchors or mooring line buoyancy elements. By making offshore operations safer, one can prevent unwanted scenarios from happening. Some of the more common unwanted consequences of loss of position or large drift are listed:

1. Loss of human life or injury
2. Hydrocarbon spill
3. Collision
4. Vessel capsizing
5. Damage to expensive equipment
6. Abortion of operation

1.3 Main Contributions

The contributions of this thesis are focused on different solutions for thruster assisted position mooring and their qualities. The roll and pitch damping control law is emphasized. Stability analyses are carried out. A Matlab Simulink model is made, and used in the analysis of the performance of the total thruster assisted position mooring system. The control system performance is also tested in model scale using the model semi-submersible CyberRig I in the Marine Cybernetics Laboratory at NTNU.

- Previous scientific work on the topic is reviewed
- The roll and pitch damping controller is studied
- Lyapunov stability analysis is performed for the RPD control law
- A setpoint chasing algorithm based on a structural reliability criterion is reviewed
- A nonlinear feedback control law based on the same reliability criterion is reviewed
- A simulation model is developed, including vessel, mooring system and a position mooring control system
- Model tests are carried out using the model semi-submersible CyberRig I
- The steady tilt phenomena for regular waves was detected during model tests

1.4 Outline of the Thesis

This Master's Thesis is built up around the modelling, simulation and model scale testing of thruster assisted position mooring systems.

Chapter 2: The mathematical modelling of the vessel, the mooring system and the environmental forces is carried out. The low-frequency model and the low-frequency environmental loads are emphasized in the modelling process. The data used in the full scale simulation model is scaled up from the data available for CyberRig I.

Chapter 3: The chapter on control system design is entitled to the different control algorithms available for thruster assisted position mooring systems. Roll and pitch damping, a setpoint chasing algorithm, and a backstepping control law are included.

Chapter 4: This chapter presents the simulation and model test set-up and results. Simulations and model tests are performed for two cases; open-loop and closed loop with PID and RPD controllers.

Chapter 5: Discussion and comparison of the simulation results and the model test results relative to theory are included.

Chapter 6: The concluding remarks are made, summarizing the main contributions of this Master's Thesis. Suggestions for further work are proposed.

Chapter 2

Mathematical Modelling

The quality of a thruster assisted position mooring system can not be sufficiently determined by static analyses alone. This is because a moored rig operating in the North Sea is a highly dynamic system. To perform a qualitative verification of the thruster assisted position mooring system, high-fidelity models, statistics, real-time simulations, and model tests needs to be applied.

2.1 Kinematics

The study of dynamics can be parted in two, kinematics and kinetics. Kinematics define the geometrical aspects of the dynamics, while kinetics consider the forces and moments that create the dynamic behaviour.

2.1.1 Degrees of Freedom

The dynamics are modelled using position and velocity vectors as defined in Fossen (2011). The first three degrees of freedom (DOF) in each vector, (2.1a) and (2.1b), represent the translational motions, while the rest represent rotational motion.

$$\boldsymbol{\eta} = \begin{bmatrix} \mathbf{p} \\ \boldsymbol{\Theta} \end{bmatrix} = [x, y, z, \phi, \theta, \psi]^T, \tag{2.1a}$$

$$\boldsymbol{\nu} = \begin{bmatrix} \mathbf{v} \\ \boldsymbol{\omega} \end{bmatrix} = [u, v, w, p, q, r]^T. \tag{2.1b}$$

For the horizontal control problem, only the horizontal degrees of freedom are considered. For these problems, yet another set of vectors is defined:

$$\boldsymbol{\eta}_h = \begin{bmatrix} x \\ y \\ \psi \end{bmatrix} = \begin{bmatrix} \mathbf{p}_h \\ \psi \end{bmatrix}, \quad \boldsymbol{\nu}_h = \begin{bmatrix} u \\ v \\ r \end{bmatrix} = \begin{bmatrix} \mathbf{v}_h \\ r \end{bmatrix}. \tag{2.2}$$

2.1.2 Reference Frames

The reference frames used are the Earth-fixed reference frame, and the body-fixed reference frame.

Earth-Fixed Reference Frame

The Earth-fixed reference frame is in this case equal to the North-East-Down (NED) frame. This reference frame is tangential to the Earth's surface with the z-axis pointing downward normal to the Earth's surface, the x-axis pointing towards the true North and the y-axis pointing toward the true East. The NED-frame is usually expressed in terms of $\{n\} = (x_n, y_n, z_n)$ with origin o_n, but it can also be expressed in terms of latitude and longitude. The position vector $\boldsymbol{\eta}$ is defined in NED-coordinates.

The Body-Fixed Reference Frame

The body-fixed reference frame is a coordinate system moving with the body. The reference system is defined as $\{b\} = (x_b, y_b, z_b)$ with origin o_b, which is usually located in the horizontal midpoint in the waterline. The velocity vector $\boldsymbol{\nu}$ is defined in body coordinates. The motions of the vessel in the body reference frame are defined in Figure 2.1.

The Frame Relation

The 6 DOF relation kinematic equations are stated in Equation 2.3. The kinematic equations relate the body frame and the earth frame through the transformation matrix.

$$\dot{\boldsymbol{\eta}} = \begin{bmatrix} \dot{\boldsymbol{p}} \\ \dot{\boldsymbol{\Theta}} \end{bmatrix} = \begin{bmatrix} \mathbf{J}_1(\boldsymbol{\Theta}) & \mathbf{0}_{3\times3} \\ \mathbf{0}_{3\times3} & \mathbf{J}_2(\boldsymbol{\Theta}) \end{bmatrix} \begin{bmatrix} \mathbf{v} \\ \boldsymbol{\omega} \end{bmatrix} = \mathbf{J}(\boldsymbol{\Theta})\boldsymbol{\nu} \tag{2.3}$$

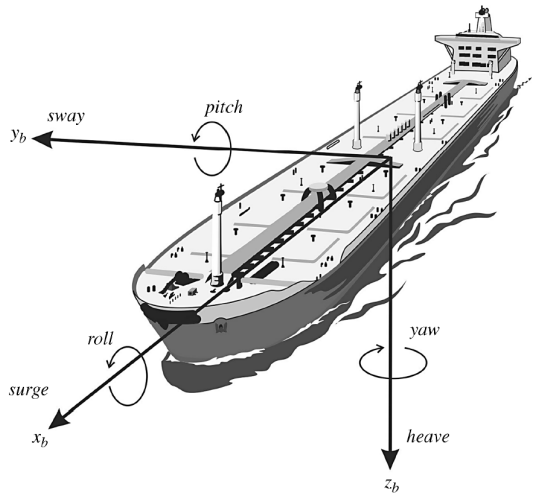

Figure 2.1: 6 DOF motions, Fossen (2011).

The principal rotation matrices, $\mathbf{J}_1(\mathbf{\Theta})$ and $\mathbf{J}_2(\mathbf{\Theta})$ can be stated as

$$\mathbf{J}_1(\mathbf{\Theta}) = \begin{bmatrix} c\psi c\theta & -s\psi c\phi + c\psi s\theta s\phi & s\psi s\phi + c\psi c\phi s\theta \\ s\psi c\theta & c\psi c\phi + s\psi s\theta s\phi & -c\psi s\phi + s\psi c\phi s\theta \\ -s\theta & c\theta s\phi & c\theta c\phi \end{bmatrix}, \tag{2.4a}$$

$$\mathbf{J}_2(\mathbf{\Theta}) = \begin{bmatrix} 1 & s\phi c\theta & c\phi t\theta \\ 0 & c\phi & -s\phi \\ 0 & s\phi/c\theta & c\phi/c\theta \end{bmatrix}, \quad \forall \theta \neq \pm\frac{\pi}{2}, \tag{2.4b}$$

where $c(\cdot) = \cos(\cdot)$, $s(\cdot) = \sin(\cdot)$ and $t(\cdot) = \tan(\cdot)$. $\mathbf{J}_1(\mathbf{\Theta})$ and $\mathbf{J}_2(\mathbf{\Theta})$ are the linear velocity transformation matrix and the angular velocity transformation matrix, respectively. $\mathbf{J}(\mathbf{\Theta})$ is the total transformation matrix.

Since the guidance system, see Section 3.1, operates only in the horizontal plane, a horizontal rotation matrix is defined too. A matrix which relates the horizontal reference frames is needed:

$$\dot{\boldsymbol{\eta}}_h = \mathbf{R}(\psi)\boldsymbol{\nu}_h \quad \Rightarrow \quad \mathbf{R}(\psi) = \begin{bmatrix} \cos\psi & -\sin\psi & 0 \\ \sin\psi & \cos\psi & 0 \\ 0 & 0 & 1 \end{bmatrix} \tag{2.5}$$

Here, $\mathbf{R}(\psi)$ is the horizontal rotation matrix.

Small angles of rotation

The transformation matrices can be simplified for small angles of rotation, $\boldsymbol{\eta}_2 = \delta\boldsymbol{\Theta}$. For the moored semi-submersible, the angular rotations will all be small even in yaw, due to the restoring forces of the mooring system. The reduced transformation matrices are reduced as in Equation (2.6) from Fossen (2011). The total transformation matrix is positive definite for small angles of rotation, that is, the eigenvalues of $\mathbf{J}(\delta\boldsymbol{\Theta})$ are strictly positive.

$$\mathbf{J}_1(\delta\boldsymbol{\Theta}) = \begin{bmatrix} 1 & -\delta\psi & \delta\theta \\ \delta\psi & 1 & -\delta\phi \\ -\delta\theta & \delta\phi & 1 \end{bmatrix} \tag{2.6a}$$

$$\mathbf{J}_2(\delta\boldsymbol{\Theta}) = \begin{bmatrix} 1 & 0 & \delta\theta \\ 0 & 1 & -\delta\phi \\ 0 & \delta\phi & 1 \end{bmatrix} \tag{2.6b}$$

$$\mathbf{J}(\delta\boldsymbol{\Theta}) = \begin{bmatrix} \mathbf{J}_1(\delta\boldsymbol{\Theta}) & \mathbf{0}_{3\times3} \\ \mathbf{0}_{3\times3} & \mathbf{J}_2(\delta\boldsymbol{\Theta}) \end{bmatrix} \tag{2.6c}$$

2.2 Modelling of the Environment

The rig is assumed to operate in the North Sea. Operations in this area involves harsh weather, especially during autumn and winter, and shallow depths. Because of the high probability of harsh weather, the PM system must designed to handle largely varying weather conditions in a reliable fashion. The fact that shallow depths can be assumed, $h < 600[m]$, lowers the requirements on the passive mooring system.

Harsh weather includes waves with high significant wave heigth, strong current, wind and wind-generated waves and currents. Environmental parameters used in the simulations are stated in Appendix B. An outline of the forces working on the rig can be seen in Figure 2.2.

2.2.1 Waves

Wave forces and moments are in theory the sum of first and second order wave-induced forces and moments. Higher order forces exist, but are assumed negligible. This is stated in Equation (2.7), see Fossen (2011).

$$\boldsymbol{\tau}_{wave} = \boldsymbol{\tau}_{wave1} + \boldsymbol{\tau}_{wave2} \tag{2.7}$$

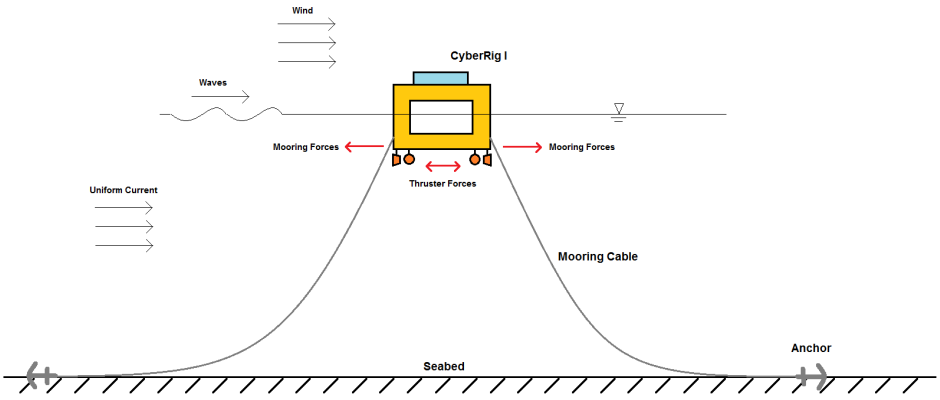

Figure 2.2: The moored rig with environmental loads.

Second-order wave drift forces, $\boldsymbol{\tau}_{wave2}$, due to short crested waves, are dominant for moored structures and will influence the low-frequency dynamics of the total system to a large extent. The first and second order wave forces and moments can be calculated using response amplitude operators (RAO).

For the simulation of waves in the North Sea, either the JONSWAP spectrum or the Torsethaugen spectrum is normally chosen. The Torsethaugen spectrum includes swell and newly generated waves, and can be found in Torsethaugen (1996). The JONSWAP spectrum is empirically described by Equation (2.8). The parameters used are typical for the North Sea; $\omega_0 = 0.8$ [s], $\gamma = 3.3$, and $H_s = 5$ [m]. The JONSWAP spectrum, along with some other well-used spectra, are represented in Figure 2.3.

$$S(\omega) = 155\frac{H_s^2}{T_1^4\omega^5}\exp\left(-\frac{199}{T_1^4\omega^4}\right)\gamma^Y \tag{2.8a}$$

$$Y = \exp\left[-\left(\frac{0.191\omega T_1 - 1}{\sqrt{2}\sigma}\right)^2\right] \tag{2.8b}$$

$$\sigma = \begin{cases} 0.07 & \text{for} \quad \omega \leq 5.24/T_1 \\ 0.09 & \text{for} \quad \omega < 5.24/T_1 \end{cases} \tag{2.8c}$$

$$T_1 = 0.834T_0 = 1.073T_z \tag{2.8d}$$

The wave forces are calculated from the waves created according to the wave spectrum. The wave height is calculated as in Equation (2.9).

$$\zeta = A = \sum_{k=1}^{N} A_k \cos(\omega_k + \varepsilon_k) = \sum_{k=1}^{N} \sqrt{2S(\omega_k)\Delta\omega}\cos(\omega_k + \varepsilon_k) \tag{2.9}$$

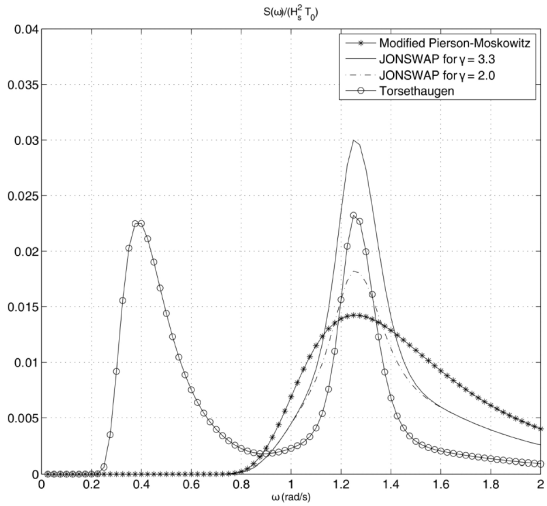

Figure 2.3: Some of the spectra available, Fossen (2011).

Both the linear and second order wave forces for degree of freedom number i can be calculated from Equation (2.10). The Newman approximation is used for the second order wave forces. The approximation is only valid for the study of low frequency dynamics because it creates additional non-physical high frequency effects. Since the rig is moored and relatively stationary when anchored, the frequency of encounter is set equal to the wave frequency: $\omega_e = \omega$.

$$\tau^i_{wave1} = \sum_{k=1}^{N} \rho g |F^i_{wave1}(\omega_k)| A_k \cos(\omega_k t + \varepsilon_k) \tag{2.10a}$$

$$= \sum_{k=1}^{N} \sqrt{2S(\omega_k)} \cos(\omega_k t + \varepsilon_k) \tag{2.10b}$$

$$\tau^i_{wave2} = 2 \left(\sum_{k=1}^{N} \sqrt{T^{ic}_{kk}} A_k \cos(\omega_k t + \varepsilon_k) \right)^2 \tag{2.10c}$$

2.2.2 Wind

Wind is a source of low frequency excitation and is implemented in the process plant model through $\boldsymbol{\tau}_{wind}$, see Equation (3.20).

$$\boldsymbol{\tau}_{wind} = \frac{1}{2}\rho_a V_{rw}^2 \begin{bmatrix} C_X(\gamma_{rw})A_{Fw} \\ C_Y(\gamma_{rw})A_{Lw} \\ C_Z(\gamma_{rw})A_{Fw} \\ C_K(\gamma_{rw})A_{Lw}H_{Lw} \\ C_M(\gamma_{rw})A_{Fw}H_{Fw} \\ C_N(\gamma_{rw})A_{Lw}L_{oa} \end{bmatrix} \tag{2.11}$$

For a semisubmercible, both pitch and roll wind forces needs to be considered in addition to the horizontal wind forces. This is due to the large areas exposed above the sea surface. In Equation (3.20), V_{rw} is the absolute relative wind speed, γ_{rw} is the angle of attack, A_{Fw} and A_{Lw} are the projected areas, and H_{Fw} and H_{Lw} are the centers of the wind exposed areas above the water line. For semisubmersibles, the wind force functions $\{C_X, \ldots, C_N\}$ for huge floating ocean structures proposed by Kitamura, Sato, Shimada, and Mikami (1997) can be used.

2.2.3 Current

Current is another type of slowly varying motion which contributes to low frequency motions. The current forces are directly integrated in the system dynamics by use of the relative velocity vector:

$$\boldsymbol{\nu}_r = \begin{bmatrix} u - u_c & v - v_c & w & p & q & r \end{bmatrix}^T. \tag{2.12}$$

The relative velocity vector is implemented in the system matrices, taking the effects of current on the system dynamics into account.

2.3 Modelling of the Mooring System

The mooring system is subject to three types of excitation, according to Triantafyllou (1990); large amplitude low frequency (LF) motion, medium amplitude wave frequency (WF) motions, and small amplitude very high frequency (HF) vortex induced vibrations. In the design of position mooring systems, only the low-frequency motions are considered. The low frequency approach is in accordance with the control system objectives in this Master's Thesis

2.3.1 Mooring Cable PDE

The partial differential equation (PDE) for cable dynamics, neglecting bending and torsional stiffness, is stated in (2.13), see Aamo and Fossen (2001).

$$\rho_0 \frac{\partial \mathbf{v}(t,s)}{\partial t} = \frac{\partial}{\partial t}(T(t,s)\mathbf{t}(t,s)) + \mathbf{f}(t,s)(1+e(t,s)), \tag{2.13}$$

where t is the time variable, $s \in [0, L]$ is the distance along the unstretched cable, from anchor to vessel, $\mathbf{v} : [t_0, \infty) \times [0, L]$ is the velocity vector, and $\mathbf{t}$ is the tangential vector. L is the length of the unstretched cable, ρ_0 is the mass per unstretched unit length of cable, $T : [t_0, \infty) \times [0, L]$ is tension, $e : [t_0, \infty) \times [0, L]$ is strain and $\mathbf{f}$ is the sum of external forces acting on the unstretched cable. The accurateness of the solution increases with node number, but so does also the computational time needed to solve the integral.

The cable is divided into several segments and nodes to keep the integral simple, as seen in Figure 2.4. In Sørensen (2013a), is was shown that a node number of ≥ 10 gives an adequat form for the mooring line forces to be estimated.

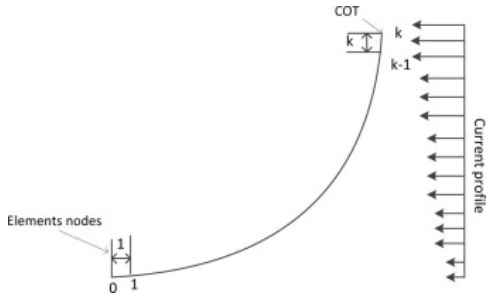

Figure 2.4: The FEM mooring model.

The external forces $\mathbf{f}$ acting on the cable are the sum of gravity and hydrostatic buouancy forces $\mathbf{f}_{(hg)}$, tangential and normal hydrodynamic drag $\mathbf{f}_{(dt)}, \mathbf{f}_{(dn)}$, and hydrodynamic inertia forces $\mathbf{f}_{(mn)}$:

$$\mathbf{f} = \mathbf{f}_{(hg)} + \mathbf{f}_{(dt)} + \mathbf{f}_{(dn)} + \mathbf{f}_{(mn)}. \tag{2.14}$$

The gravity and hydrostatic forces are modelled according to

$$\mathbf{f}_{(hg)} = \rho_0 \frac{\rho_c - \rho_w}{(1+e)\rho_c}\mathbf{g}, \tag{2.15}$$

where $\mathbf{g}$ is the gravitational acceleration, ρ_c is the cable density, and ρ_w is the surrounding water density. The hydrodynamic drag forces are modelled according to Morison's

equation:

$$\mathbf{f}_{(dt)} = -\frac{1}{2} C_{D,t} D \rho_w |\mathbf{v}_t| \mathbf{v}_t \tag{2.16a}$$

$$\mathbf{f}_{(dn)} = -\frac{1}{2} C_{D,n} D \rho_w |\mathbf{v}_n| \mathbf{v}_n \tag{2.16b}$$

In (2.16), the forces are the tangential and normal hydrodynamic drag forces respectively. Here, $\mathbf{v}_t$ is the tangential velocity, $\mathbf{v}_n$ is the normal velocity, $C_{D,t}$ is the tangential drag coefficient, $C_{D,n}$ is the normal drag coefficient and D is the unstretched cable diameter. The hydrodynamic added inertia force is described as

$$\mathbf{f}_{(mn)} = -C_A \rho_w \frac{\pi D^2}{4} \mathbf{a}, \tag{2.17}$$

where C_A is the hydrodynamic mass coefficient, and $\mathbf{a} : [t_0, \infty) \times [0, L]$ is the acceleration.

By compairing the diameter of the mooring line, which is in the order of 0.1 (m), to the wave height, it is found that viscous forces will dominate for wave heights larger than 1 (m), see Faltinsen (1990). This means added mass can be neglected for rough sea states, which are defined to have larger significant wave height and higher wind speeds. But for the study of deep sea mooring, $h > 600$ (m), added mass needs to be considered.

In the PDE, a position vector $\mathbf{r} : [t_0, \infty) \times [0, L]$ is introduced, such that $\mathbf{t} = \frac{1}{1+e} \frac{\delta \mathbf{r}}{\delta s}$. Equation (2.13) can now be written

$$\rho_0 \frac{\partial^2 \mathbf{r}}{\partial t^2} = \frac{\partial}{\partial s} \left(\frac{T}{1+e} \frac{\partial \mathbf{r}}{\partial s} \right) + \mathbf{f}(1+e). \tag{2.18}$$

Introducing *Hooke's law* yields

$$\rho_0 \frac{\partial^2 \mathbf{r}}{\partial t^2} = \frac{\partial}{\partial s} \left(E A_0 \frac{e}{1+e} \frac{\partial \mathbf{r}}{\partial s} \right) + \mathbf{f}(1+e). \tag{2.19}$$

E is Young's modulus of elasticity, and A_0 is the cross-sectional area of the unstreched cable.

Discretization into finite elements is done using the Galerkin method. The generalized problem can be stated as

$$\int_0^L \left(\rho_0 \frac{\partial^2 \mathbf{r}}{\partial t^2} - \frac{\partial}{\partial s} \left(E A_0 \frac{e}{1+e} \frac{\partial \mathbf{r}}{\partial s} \right) + \mathbf{f}(1+e) \right) \cdot \mathbf{w} \, ds = 0. \tag{2.20}$$

In Equation (2.20), $\mathbf{w}$ is a trial function used in the discretization. The trial function is a linear combination of the basis functions. Basis functions are defined to be different modes of deflection, or shapes, that the slender structure can have under impact from external forces.

2.3.2 Mooring Configuration

A vessel can be turret moored or spread moored. For turret mooring, the anchor lines are fastened to a circular turret installed at some point along the centerline of the vessel, often close to the bow. The vessel is free to rotate around the turret and weathervaning can be used to control the heading. Turret mooring is prefered for long and slim vessels and other vessels that can take advantage of weathervaning. Spread mooring systems have widely allocated mooring points on the vessel, constraining the vessel from rotation about its vertical axis. For vessels which are nearly as wide as they are long, weathervaning is not contributing to stationkeeping anyhow.

2.3.3 Mooring Cable Implementation

The described mooring line model is developed by Aamo and Fossen (2001) and implemented in a Simulink FEM model block. One block represents one mooring cable and calculates the forces with respect to the mooring point position, current velocity, cable velocity and depth. The calculations are performed fairly quickly, allowing the rest of the simulation model to be accurate and also ensure relatively short simulation time.

The mooring forces are calculated for several mooring lines in a spread moored system in the NED coordinate system. The forces are mainly dependent of the horizontal distance between the anchor and the mooring point on the rig. The forces are then converted to body coordinates through the transformation presented in Equation (2.21), as proposed by Faltinsen (1990).

$$\boldsymbol{\tau}_{moor} = \sum_{i=1}^{N} T_i \begin{bmatrix} \cos\alpha_i \\ \sin\alpha_i \\ (\bar{x}_i \sin\alpha_i - \bar{y}_i \cos\alpha_i) \end{bmatrix} \tag{2.21}$$

Here, α_i is the relative angle between the rig heading and the horizontal direction of the mooring force for mooring line i, and T_i is the horizontal mooring force for mooring line i. $\bar{x}_i$ and $\bar{y}_i$ are the positions of the mooring points on the rig relative to the rig body coordinate system. These vectors refer to the point on the rig where the mooring forces act. The mooring forces are for simplicity only affecting the horizontal motions of the rig, which are surge, sway, and yaw.

For mooring systems at shallow depths, $h < 600$ (m), it is assumed that only a quasi-static mooring model is needed for the dynamic analysis. This is because the mooring system nonlinear dynamics are less dominant for shallow depths. By studying the responses for the nonlinear finite element method (FEM) mooring system, a mooring model linearized around the working point can be obtained. Normally the working point is the point where the sum of mooring forces is zero.

The mooring system forces can be linearized as in Equation (2.22). The linearized mooring forces can in turn be implemented in the control plant model in Section 2.4.8.

$$\boldsymbol{\tau}_{moor} = -\mathbf{J}^T(\psi)\mathbf{g}_{mo}(\boldsymbol{\eta}) - \mathbf{d}_{mo}(\boldsymbol{\nu}) \tag{2.22a}$$

$$\approx -\mathbf{J}^T(\psi)\mathbf{G}_{mo}\boldsymbol{\eta} - \mathbf{D}_{mo}\boldsymbol{\nu} \tag{2.22b}$$

The linearization is performed by partial derivation, see Equation (2.23).

$$\mathbf{G}_{mo} = \left.\frac{\partial \mathbf{g}_{mo}}{\partial \boldsymbol{\eta}}\right|_{\boldsymbol{\eta}=\boldsymbol{\eta}_0}, \quad \mathbf{D}_{mo} = \left.\frac{\partial \mathbf{d}_{mo}}{\partial \boldsymbol{\nu}}\right|_{\boldsymbol{\nu}=\mathbf{0}}. \tag{2.23}$$

2.4 Modelling of the Rig Kinetics

The kinetics of a system connects the forces and moments to the motions of a system.

2.4.1 Rigid Body Forces and Moments

The forces and moments acting on the system are in equilibrium with the rigid body forces and moments resulting from rigid body motion. This satisfies the Newton-Euler Equations of Motion, Fossen (2011). The equilibrium can be stated according to

$$\mathbf{M}_{RB}\dot{\boldsymbol{\nu}} + \mathbf{C}_{RB}(\boldsymbol{\nu})\boldsymbol{\nu} = \boldsymbol{\tau}_{RB}, \tag{2.24}$$

where $\mathbf{M}_{RB}$ is the rigid body mass matrix, $\mathbf{C}_{RB}$ is the rigid body Coriolis and centripetal matrix due to rotations about the inertial frame, $\boldsymbol{\eta}$ and $\boldsymbol{\nu}$ are stated in Section 2.1.1, and $\boldsymbol{\tau}_{RB}$ is the generalized vector of external forces and moments in body coordinates. The rigid body matrices can be stated

$$\mathbf{M}_{RB} = \begin{bmatrix} m\mathbf{I}_{3\times 3} & -m\mathbf{S}(\mathbf{r}_g) \\ m\mathbf{S}(\mathbf{r}_g) & \mathbf{I}_b \end{bmatrix} \tag{2.25a}$$

$$\mathbf{C}_{RB}(\boldsymbol{\nu}) = \begin{bmatrix} m\mathbf{I}_{3\times 3} & -m\mathbf{S}(\boldsymbol{\omega})\mathbf{S}(\mathbf{r}_g) \\ m\mathbf{S}(\mathbf{r}_g)\mathbf{S}(\boldsymbol{\omega}) & -\mathbf{S}(\mathbf{I}_b\boldsymbol{\omega}) \end{bmatrix} \tag{2.25b}$$

where m is the vessel mass, $\mathbf{I}_b$ is the vessel inertia forces, $\mathbf{S}(\cdot)$ is the cross product operator as stated in Fossen (2011), and $\mathbf{I}_{3\times 3}$ is a 3×3 identity matrix. The vector $\mathbf{r}_g$ defines the distance from the origin to the center of gravity. In the case where the center of gravity is placed in the geometric horizontal center in the waterplane, $\mathbf{r}_g$ is equal to zero.

2.4.2 Hydrodynamic Forces and Moments

The hydrodynamic forces and moments, $\boldsymbol{\tau}_{hyd}$, are dependent on the relative velocity vector presented in Section 2.2.3.

$$\boldsymbol{\tau}_{hyd} = -\mathbf{M}_A\dot{\boldsymbol{\nu}}_r - \mathbf{C}_A(\boldsymbol{\nu}_r)\boldsymbol{\nu}_r - \mathbf{D}_L\boldsymbol{\nu}_r - \mathbf{D}_{NL}(\boldsymbol{\nu}_r)\boldsymbol{\nu}_r \tag{2.26}$$

In Equation (2.26), the matrix $\mathbf{M}_A$ is the hydrodynamic added mass matrix, $\mathbf{C}_A(\boldsymbol{\nu}_r)$ is the hydrodynamic Coriolis and centripetal matrix, $\mathbf{D}_L$ is the linear hydrodynamic damping matrix, and $\mathbf{D}_{NL}(\boldsymbol{\nu}_r)$ is the nonlinear hydrodynamic damping matrix.

2.4.3 Hydrostatic Forces and Moments

The hydrostatic forces and moments are equal to the buoyancy and gravity effects causing restoring forces and moments in heave, roll and pitch. Since these three DOFs are decoupled, we will have no coupled restoring forces. The only restoring forces are restoring in heave due to heave motions, $-Z_z$, a restoring moment in roll due to roll motion, $-K_\phi$, and a restoring moment in pitch due to pitch motion, $-M_\theta$. Assuming small rotations and knowing that the vessel is vertical sides in the waterline, one can write

$$\begin{aligned}\mathbf{G} &= diag\{0, 0, -Z_z, -K_\phi, -M_\theta, 0\} \\ &= diag\{0, 0, \rho g A_{wp}(0), \rho g \nabla \overline{GM}_T, \rho g \nabla \overline{GM}_L, 0\},\end{aligned} \tag{2.27}$$

where ρ is the water density, g is the gravitational acceleration, $A_{wp}(0)$ is the vessel horizontal area in the water plane, ∇ is the displacement of the vessel, $\overline{GM}_T$ and $\overline{GM}_L$ are the transverse and longitudinal metacentric heights, respectively.

2.4.4 Forces and Moments Due to the Mooring System

The passive mooring system has characteristic low eigenfrequencies and slow horizontal dynamics. That means that the horizontal motions are excited only for low frequency wave loads, that is, the second order LF wave forces.

Since the rig has a spread mooring system, which means the mooring lines are attached at distributed points on the rig, preferably the rig corners, the mooring system will impose a yaw moment on the rig in addition to forces in surge and sway. This is the main difference between turret moored and spread moored mooring systems. For a spread moored rig, the low-frequency yaw dynamics as imposed by the mooring system needs to be considered. The mooring forces, $\boldsymbol{\tau}_{moor}$, in the rigid body equations of motion are defined as in Equation (2.21).

2.4.5 Thruster Dynamics

The dynamics of each single thruster can be stated as in Smogeli et al. (2005).

$$\dot{Q}_m = \frac{1}{T_m}(Q_c - Q_m) \tag{2.28a}$$
$$I_s\dot{\omega} = Q_m - Q_a - Q_f(\omega) \tag{2.28b}$$
$$Q_a = f_Q(\theta_m, \xi_m) \tag{2.28c}$$
$$T_a = f_T(\theta_m, \xi_m) \tag{2.28d}$$
$$P_a = Q_a\omega \tag{2.28e}$$

The thruster characteristics in Equation (2.28) are described by the following set of parameters; the motor time constant T_m, the commanded torque Q_c, the motor torque Q_m, the rotational intertia of the propeller including added mass I_s, the shaft friction $Q_f(\omega)$, where ω is the rotational speed of the propeller, the propeller load torque Q_a, the propeller thrust T_a, and finally, the propeller power P_a. f_Q and f_T are general functions dependent of fixed thruster parameters θ_m, and variable thruster parameters ξ_m.

The shaft friction is often assumed to be linear and the thrust and torque dynamics are modelled using quadratic thruster characteristics:

$$T_a = K_T\rho D^4|n|n, \tag{2.29a}$$
$$Q_a = K_Q\rho D^5|n|n, \tag{2.29b}$$

where K_T and K_Q are the thrust and torque coefficients, ρ is the water density, D is the propeller diameter, and n is the rotational speed of the propeller in [RPM].

2.4.6 Control Allocation

The thrusters will, in the same manner as the mooring lines, operate in distributed positions, creating moments about the rig's center of gravity. The thrusters are installed below the rig bottom and the rig is deeply submerged during most stationary operations, including position mooring. Therefore, the thrusters will contribute with forces and moments in surge, sway, roll, pitch, and yaw.

$$\boldsymbol{\tau}_{thr} = \mathbf{T}(\boldsymbol{\alpha})\mathbf{K}\mathbf{u} \tag{2.30}$$

Equation (2.30) shows that the thruster force is a function of the actuator configuration matrix, a efficiency/loss coefficient matrix $\mathbf{K}$, and the control input vector $\mathbf{u}$. The actuator configuration matrix $\mathbf{T}(\boldsymbol{\alpha})$ can be defined as a set of column vectors as in Equation (2.31),

see Tyssø and Aga (2006).

$$\mathbf{T}(\boldsymbol{\alpha}) = [\mathbf{t}_1, \mathbf{t}_2, \ldots, \mathbf{t}_r] = \begin{bmatrix} \cos\alpha_1 & \ldots & \cos\alpha_r \\ \sin\alpha_1 & \ldots & \sin\alpha_r \\ 0 & \ldots & 0 \\ -l_{z_1}\sin\alpha_1 & \ldots & -l_{z_r}\sin\alpha_r \\ l_{z_1}\cos\alpha_1 & \ldots & l_{z_r}\cos\alpha_r \\ l_{x_1}\sin\alpha_1 - l_{y_1}\cos\alpha_1 & \ldots & l_{x_r}\sin\alpha_r - l_{y_r}\cos\alpha_r \end{bmatrix} \tag{2.31}$$

Here, $\alpha_i, i = 1..r$ is the thruster angle for thruster i, and $l_{x_i}, l_{y_i}, l_{z_i}$ are the thruster position coordinates relative to the body coordinate system. The submerged depth l_{z_i} is the same for all thrusters; $\{l_{z_1}, \ldots, l_{z_r}\} = l_z$.

2.4.7 The Process Plant Model

The nonlinear 6 DOF low-frequency process plant model can according to Sørensen (2013a) be stated

$$\begin{aligned} \mathbf{M}_{RB}\dot{\boldsymbol{\nu}} + \mathbf{M}_A\dot{\boldsymbol{\nu}}_r + \mathbf{C}_{RB}(\boldsymbol{\nu})\boldsymbol{\nu} + \mathbf{C}_A(\boldsymbol{\nu}_r)\boldsymbol{\nu}_r & \\ + \mathbf{D}_L\boldsymbol{\nu}_r + \mathbf{D}_{NL}(\boldsymbol{\nu}_r)\boldsymbol{\nu}_r + \mathbf{G}\boldsymbol{\eta} & \qquad (2.32a) \\ = \boldsymbol{\tau}_{wind} + \boldsymbol{\tau}_{wave2} + \boldsymbol{\tau}_{thr} + \boldsymbol{\tau}_{moor}, & \\ \dot{\boldsymbol{\eta}} = \mathbf{J}^T(\boldsymbol{\Theta})\boldsymbol{\nu}. & \qquad (2.32b) \end{aligned}$$

The relations, matrices and parameters used in Equation (2.32) are defined in Section 2.1.1 to Section 2.4.6.

2.4.8 The Control Plant Model

The control plant model is the simplified model used for design of the control system. Only the physics that are most crucial for the controller design are included.

A Markov Process bias model is used

$$\dot{\mathbf{b}} = -{\mathbf{T_b}}^{-1}\mathbf{b} + \mathbf{E}_b\mathbf{w}_b, \tag{2.33}$$

which is needed to prove the nonlinear passive observer (NPO) globally exponentially stable in Section 3.3.1. In Equation (2.33), the matrices $\mathbf{T}_b$ and $\mathbf{E}_b$ reflect the bias dynamics resulting from the bias disturbance $\mathbf{w}_b$ and the actual bias $\mathbf{b}$ resulting from current, wind and second order wave drift forces. The matrix $\mathbf{T}_b$ contains the bias time constants and ensures low-pass filtering of the bias estimates.

For control purposes, it is common to divide the modelling into a LF model and a WF model. The wave frequency motion is represented by a state space model:

$$\dot{\boldsymbol{\xi}} = \mathbf{A}_w \boldsymbol{\xi} + \mathbf{E}_w \mathbf{w}_w, \tag{2.34a}$$

$$\boldsymbol{\eta}_w = \mathbf{C}_w \boldsymbol{\xi}, \tag{2.34b}$$

where $\boldsymbol{\eta}_w$ are the linear wave induced motions. The disturbance $\mathbf{w}_w$ is a zero-mean Gaussian white noise vector. The system matrices are defined

$$\mathbf{A}_w = \begin{bmatrix} \mathbf{0}_{6\times6} & \mathbf{I}_{6\times6} \\ -\boldsymbol{\Omega}^2 & -2\boldsymbol{\Lambda}\boldsymbol{\Omega} \end{bmatrix}, \tag{2.35a}$$

$$\mathbf{C}_w = \begin{bmatrix} \mathbf{0}_{6\times6} & \mathbf{I}_{6\times6} \end{bmatrix}, \tag{2.35b}$$

$$\mathbf{E}_w = \begin{bmatrix} \mathbf{0}_{6\times6} \\ \mathbf{K}_w \end{bmatrix}. \tag{2.35c}$$

In Equation (2.35), $\boldsymbol{\Omega}$ is the diagonal frequency matrix, $\boldsymbol{\Lambda}$ is the diagonal damping ration matrix, and $\mathbf{K}_w$ is the diagonal Gaussian disturbance matrix.

The LF control plant model is stated by

$$\dot{\boldsymbol{\eta}} = \mathbf{J}^T(\boldsymbol{\Theta})\boldsymbol{\nu}, \tag{2.36a}$$

$$\mathbf{M}\dot{\boldsymbol{\nu}} + \mathbf{D}\boldsymbol{\nu} + \mathbf{J}^T(\boldsymbol{\Theta})\mathbf{G}\boldsymbol{\eta} = \mathbf{J}^T(\boldsymbol{\Theta})\mathbf{b} + \boldsymbol{\tau} + \boldsymbol{\tau}_{moor}. \tag{2.36b}$$

All matrices and parameters in Equation (2.36) are earlier defined. The resulting control plant model is a gather-up of all the dynamics in the system:

$$\dot{\boldsymbol{\xi}} = \mathbf{A}_w \boldsymbol{\xi} + \mathbf{E}_w \mathbf{w}_w \tag{2.37a}$$

$$\dot{\boldsymbol{\eta}} = \mathbf{J}^T(\boldsymbol{\Theta})\boldsymbol{\nu} \tag{2.37b}$$

$$\dot{\mathbf{b}} = -\mathbf{T}_b^{-1}\mathbf{b} + \mathbf{E}_b \mathbf{w}_b \tag{2.37c}$$

$$\mathbf{M}\dot{\boldsymbol{\nu}} = -\mathbf{D}\boldsymbol{\nu} - \mathbf{J}^T(\boldsymbol{\Theta})\mathbf{G}\boldsymbol{\eta} + \mathbf{J}^T(\boldsymbol{\Theta})\mathbf{b} + \boldsymbol{\tau} + \boldsymbol{\tau}_{moor} \tag{2.37d}$$

$$\mathbf{y} = \boldsymbol{\eta} + \mathbf{C}_w \boldsymbol{\xi} + \mathbf{v} \tag{2.37e}$$

In Equation (2.37), the mass matrix $\mathbf{M}$ consist of both the rigid-body mass and the hydrodynamic added mass present in the process plant model. The vector $\mathbf{y}$ is the measurement vector from the reference system.

For the study of LF dynamics only, $\boldsymbol{\xi}$ is often neglected.

Figure 2.5: The model CyberRig I.

2.5 CyberRig I

For the purpose of analysis and simulations, a typical vessel for spread mooring is chosen. The rig model CyberRig I, as seen in Figure 2.5, is used in the physical model tests. The model is designed and developed at the Department of Engineering Cybernetics and is fit for the defined control objectives. For the analysis performed in Matlab Simulink, the rig is scaled to full scale. Full-scale calculations and simulations are the norm in scientific writing, and the results obtained will therefore be comparable to other scientific tests. The model scale parameters are given in Appendix A, while the scaling laws used are presented in Section 2.5.2.

2.5.1 System Matrices

The rigid body mass matrix along with the added mass matrix, the restoring matrix, and the linear damping matrix for CyberRig I are calculated by WAMIT and presented in Tyssø and Aga (2006). The mass matrix is diagonal, the added mass matrix has coupling effects in roll-sway and surge-pitch, and the restoring matrix has no coupling terms. The matrices

are stated in model scale in Equation (2.38).

$$\mathbf{M}_{RB} = diag\{54.93, 54.93, 54.93, 1.24, 1.24, 13.73\} \tag{2.38a}$$

$$\mathbf{M}_A = \begin{bmatrix} 21.61 & 0 & 0 & 0 & 2.55 & 0 \\ 0 & 21.61 & 0 & -2.55 & 0 & 0 \\ 0 & 0 & 70.67 & 0 & 0 & 0 \\ 0 & -2.57 & 0 & 5.09 & 0 & 0 \\ 2.57 & 0 & 0 & 0 & 5.09 & 0 \\ 0 & 0 & 0 & 0 & 0 & 2.97 \end{bmatrix} \tag{2.38b}$$

$$\mathbf{D}_L = diag\{16.15, 16.15, 0.03, 0, 0.06, 3.28\} \tag{2.38c}$$

$$\mathbf{G} = diag\{0, 0, 1.03, 0.16, 0.16, 0\} \tag{2.38d}$$

In addition, the linear and nonlinear damping in heave, roll, and pitch has been estimated through decay tests on the model semi-submersible CyberRig I. Model test results are presented in Chapter 4.

2.5.2 Scaling Laws

The scaling laws from model to full size rig are given in Steen (2012). A scaling parameter of $\lambda = 100$ [-] is assumed. The chosen scaling ratio corresponds well with the average parameters of semi-submersibles operating in the North Sea. The parameters for CyberRig I can be scaled according to

$$L_F = \lambda L_M \qquad = 100 \cdot L_M, \tag{2.39a}$$

$$m_F = \frac{\rho_F}{\rho_M}\lambda^3 m_M \qquad = 1025000 \cdot m_M, \tag{2.39b}$$

$$F_F = \frac{\rho_F}{\rho_M}\lambda^3 F_M \qquad = 1025000 \cdot F_M, \tag{2.39c}$$

$$M_F = \frac{\rho_F}{\rho_M}\lambda^4 M_M \qquad = 102500000 \cdot M_M, \tag{2.39d}$$

$$a_F = a_M \qquad = a_M, \tag{2.39e}$$

$$v_F = \sqrt{\lambda} \cdot v_M \qquad = 10 \cdot v_M, \tag{2.39f}$$

$$t_F = \sqrt{\lambda} \cdot t_M \qquad = 10 \cdot t_M, \tag{2.39g}$$

where m are mass terms, F are force terms, M are moments, a is acceleration, v is velocity, and t is time. The subscript F indicates full-scale, while subscript M indicates model-scale. Equation (2.39a) is the definition of the scaling parameter λ. All system matrices for CyberRig I can be scaled using the relations presented in Equation (2.39).

Chapter 3

Control System Design

A good control system consists of several components, and all of them need to be well-functioning and reliable, both separately and in cooperation with each other. A range of sensors and navigation systems give feedback on the state of the vessel, an observer estimates the correct states from the measured states, the filtered estimates goes into the control system and forces are acting on the vessel through the thruster system. In addition there is the human-machine interface (HMI), which allows an operator to give external input to the control system.

3.1 Position Mooring Control System

A standard control system consists of a navigation system, a control system and a guidance system, see Fossen (2011). These independent components can together fullfill the objectives of the total thruster assisted position mooring system.

The navigation system consists of the signal processing and the observer. The navigation system is responsible for the feedback on position, speed and acceleration of the vessel to the controller. The observer will also consider the output from the control allocation algorithm when estimating the motions of the vessel.

The guidance system has two components, the setpoint chasing algorithm and the reference model. The guidance system provides the desired position and velocity for the vessel, ensuring that the desired behavior is smooth.

The control system, including the Controller and the Control Allocation, receive the desired position and velocity from the guidance system, and the current position, speed and velocity from the navigation system. The controller will give a control input u to the

control allocation algorithm, which distributes the input among the thrusters installed on the vessel. The control system will try and decrease the error between the desired and current position and velocity of the vessel.

The total control system is illustrated in Figure 3.1. The different control blocks and the flow of information among them can be seen.

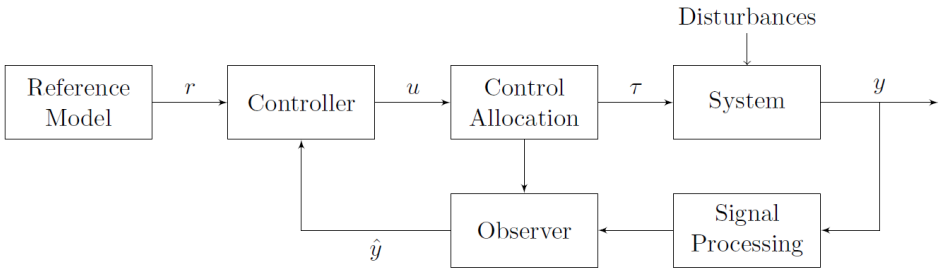

Figure 3.1: Overview of the position mooring system.

In Figure 3.1, mooring system forces and environmental forces are gathered in the disturbance term. The setpoint calculated from the setpoint chasing algorithm is input to the reference model. The controller consist of both the roll and pitch damping controller, and the model-based controller found through backstepping techniques. The nonlinear passive observer chosen for this purpose take in both the signals from the signal processing block and the input from the control allocation block. The system is the moored semi-submersible, represented by a full-scale model of CyberRig I.

3.2 Controller Objectives

The controller objectives in position mooring are first of all to make vessel stationkeeping more reliable and safe. Injuries, loss of life, and hydrocarbon spill are some of the unwanted scenarios. It is a known fact that a smart use of computational power in stationkeeping contributes to increased reliability and safety. To reduce fuel consumption and increase redundancy, the combination of mooring and DP is studied. On the control side, the main objective is to combine the mooring system and the PM algorithms so as to ensure a higher level of stationkeeping for harsh weather and at the same time utilize the restoring and damping forces of the passive mooring system.

3.3 Observer

Including an observer in the control system enables filtering and state estimation. Noisy signals will then be filtered and missing states in the available measurements can be reconstructed through state estimation. The main objectives of an observer are position and velocity estimation, bias estimation and wave filtering, see Sørensen (2013b).

3.3.1 Nonlinear Passive Observer

The idea of a nonlinear passive observer (NPO) was motivated by a wish for passivity in the observer, meaning that the observer is not introducing additional energy into the control loop, but might instead extract energy from the closed-loop system.

The NPO, as presented in Equation (3.1), was developed by Fossen and Strand (1999). The control plant model used as basis for design of the NPO is presented in Section 2.4.8. The NPO includes wave filtering, and position, velocity and bias estimation. The tuning parameters are few, and each is directly coupled to the dynamics of the controlled system. This is due to the fact that the observer is model-based by design.

$$\dot{\hat{\boldsymbol{\xi}}} = \mathbf{A}_w \hat{\boldsymbol{\xi}} + \mathbf{K}_1(\boldsymbol{\omega}_0)\tilde{\mathbf{y}} \tag{3.1a}$$

$$\dot{\hat{\boldsymbol{\eta}}} = \mathbf{J}(\boldsymbol{\Theta})\hat{\boldsymbol{\nu}} + \mathbf{K}_2\tilde{\mathbf{y}} \tag{3.1b}$$

$$\dot{\hat{\mathbf{b}}} = -\mathbf{T}^{-1}\hat{\mathbf{b}} + \mathbf{K}_3\tilde{\mathbf{y}} \tag{3.1c}$$

$$\mathbf{M}\dot{\hat{\boldsymbol{\nu}}} = -\mathbf{D}_L\hat{\boldsymbol{\nu}} - \mathbf{J}^T(\boldsymbol{\Theta})\mathbf{G}\hat{\boldsymbol{\eta}} + \mathbf{J}^T(\boldsymbol{\Theta})\hat{\mathbf{b}} + \boldsymbol{\tau} + \mathbf{J}^T(\boldsymbol{\Theta})\mathbf{K}_4\tilde{\mathbf{y}} \tag{3.1d}$$

$$\hat{\mathbf{y}} = \hat{\boldsymbol{\eta}} + \mathbf{C}_w\hat{\boldsymbol{\xi}} \tag{3.1e}$$

The nonlinear passive observer consist of a wave filter, the kinematic relation, the Markov process bias estimator, the rigid-body kinetics, and the measurement vector, respectively. Choosing the bias model to be represented by a Markov process, which means low pass filtering is implemented in the observer, $T < \infty$, yields exponential stability for the bias estimator dynamics.

3.3.2 Stability of NPO

The nonlinear passive observer in Equation (3.1) with tuned observer gain matrices is proved to be passive and globally exponentially stable using a strictly positive real (SPR) Lyapunov approach on the observer estimation errors. The observer estimation errors are

defined in Equation (3.2).

$$\tilde{\boldsymbol{\xi}} = \boldsymbol{\xi} - \hat{\boldsymbol{\xi}} \tag{3.2a}$$
$$\tilde{\boldsymbol{\eta}} = \boldsymbol{\eta} - \hat{\boldsymbol{\eta}} \tag{3.2b}$$
$$\tilde{\mathbf{b}} = \mathbf{b} - \hat{\mathbf{b}} \tag{3.2c}$$
$$\tilde{\boldsymbol{\nu}} = \boldsymbol{\nu} - \hat{\boldsymbol{\nu}} \tag{3.2d}$$

A new output vector is defined:

$$\tilde{\mathbf{z}}_0 \triangleq \mathbf{K}_4\tilde{\mathbf{y}} + \mathbf{G}\tilde{\boldsymbol{\eta}} - \tilde{\mathbf{b}} \triangleq \mathbf{C}_0\tilde{\mathbf{x}}_0, \tag{3.3}$$

where

$$\tilde{\mathbf{x}}_0 \triangleq \begin{bmatrix} \tilde{\boldsymbol{\xi}} \\ \tilde{\boldsymbol{\eta}} \\ \tilde{\mathbf{b}} \end{bmatrix}, \quad \mathbf{w} \triangleq \begin{bmatrix} \mathbf{w}_w \\ \mathbf{w}_b \end{bmatrix}. \tag{3.4}$$

The error dynamics can now be written in compact form:

$$\mathbf{M}\dot{\tilde{\boldsymbol{\nu}}} = -\mathbf{D}\tilde{\boldsymbol{\nu}} - \mathbf{J}^T(\boldsymbol{\Theta})\mathbf{C}_0\tilde{\mathbf{x}}_0 \tag{3.5a}$$
$$\dot{\tilde{\mathbf{x}}}_0 = \mathbf{A}_0\tilde{\mathbf{x}}_0 + \mathbf{B}_0\mathbf{J}(\boldsymbol{\Theta})\tilde{\boldsymbol{\nu}} + \mathbf{E}_0\mathbf{w} \tag{3.5b}$$

By introducing new error terms,

$$\varepsilon_z \triangleq -\mathbf{J}^T(\boldsymbol{\Theta})\tilde{\mathbf{z}}_0, \quad \varepsilon_\nu \triangleq \mathbf{J}(\boldsymbol{\Theta})\tilde{\boldsymbol{\nu}}, \tag{3.6}$$

a storage function is presented

$$S_1 = \frac{1}{2}\tilde{\boldsymbol{\nu}}^T\mathbf{M}\tilde{\boldsymbol{\nu}} > 0. \tag{3.7}$$

The time derivative of the storage function is calculated

$$\dot{S}_1 = -\frac{1}{2}\tilde{\boldsymbol{\nu}}^T(\mathbf{D} + \mathbf{D}^T)\tilde{\boldsymbol{\nu}} + \tilde{\boldsymbol{\nu}}^T\varepsilon_z, \tag{3.8}$$

which yields

$$\tilde{\boldsymbol{\nu}}^T\varepsilon_z \geq \dot{S}_1 + \tilde{\boldsymbol{\nu}}^T\mathbf{D}\tilde{\boldsymbol{\nu}}. \tag{3.9}$$

According to Definition 6.3 in Khalil (2002), the mapping $\varepsilon_z \mapsto \tilde{\boldsymbol{\nu}}$ is state strictly passive.

Passivity and stability of the total error dynamics of the NPO can be proved if the observer gain matrices are chosen such that the observer error dynamics satisfy the Kalman-Yakubovich-Popov (KYP) Lemma, which corresponds to Lemma 6.3 in Khalil (2002). The KYP-Lemma is fullfilled if the matrix $\mathbf{A}_0$ is Hurwitz, the error dynamics are observable and controllable, and there exists matrices $\mathbf{P} = \mathbf{P}^T > 0$ and $\mathbf{Q} = \mathbf{Q}^T > 0$

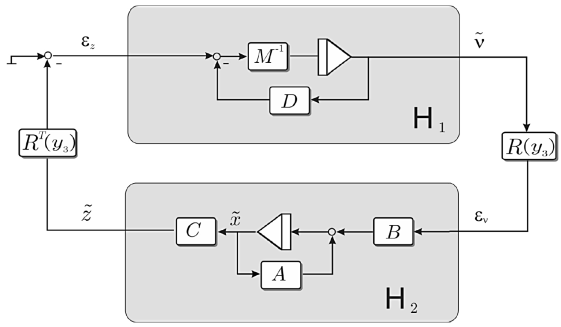

Figure 3.2: Block diagram of the error dynamics, Fossen (2011).

such that

$$\mathbf{P}\mathbf{A_0} + \mathbf{A_0^T}\mathbf{P} = -\mathbf{Q}, \tag{3.10a}$$

$$\mathbf{B_0^T}\mathbf{P} = \mathbf{C_0}. \tag{3.10b}$$

The stability of the system is only valid for decoupled systems. The tuning matrices are therefore decoupled and diagonal. The transfer functions for each degree of freedom are studied and plotted in bode plots. The transfer functions are gathered in a diagonal matrix

$$\mathbf{H}(s) = \text{diag}\{h_1(s), \cdots, h_2(s)\} \tag{3.11}$$

connecting the error vectors

$$\tilde{\mathbf{z}}(s) = \mathbf{H}(s)\boldsymbol{\varepsilon}_\nu(s) = \mathbf{H}_0(s)\mathbf{H}_B(s)\boldsymbol{\varepsilon}_\nu(s) \tag{3.12}$$

where

$$\mathbf{H}_0(s) = \mathbf{C}_0[s\mathbf{I} + \mathbf{A}_0 - \mathbf{K}_0(\boldsymbol{\omega_0})\mathbf{C}_0]^{-1}\mathbf{B}_0 \tag{3.13a}$$

$$\mathbf{H}_B(s) = \mathbf{K}_4 + (s\mathbf{I} + \mathbf{T}^{-1})^{-1}\mathbf{K}_3 \tag{3.13b}$$

To be able to filter out the first order wave motions, the transfer functions h_{0i} of the error dynamics must have a given form. This form is given by yet another transferfunction:

$$h_{di}(s) = \frac{s^2 + 2\lambda_i\omega_{0i}s + \omega_{0i}^2}{(s^2 + 2\zeta_{ni}\omega_{0i}s + \omega_{0i}^2)(s + \omega_{ci})} \tag{3.14}$$

To obtain the desired form for h_{0i} , the following tuning rules are proposed:

$$K_{1i}(\omega_{0i}) = -2(\zeta_{ni} - believed\lambda_i)\frac{\omega_{ci}}{\omega_{0i}} \tag{3.15a}$$

$$K_{1(i+3)}(\omega_{0i}) = 2\omega_{0i}(\zeta_{ni} - \lambda_i) \tag{3.15b}$$

$$K_{2i} = \omega_{ci} \tag{3.15c}$$

Regaring the remaining tuning parameters, the rule

$$\frac{1}{T_i} < \frac{K_{3i}}{K_{4i}} < \omega_{oi} < \omega_{ci} \tag{3.16}$$

is used to ensure passive estimation. In Equation (3.16), T_i is the low pass bias filtering term, ω_{oi} is the response frequency, and ω_{ci} is the cut-off frequency. The term K_{3i} should be sufficiently high to ensure proper bias estimation.

The NPO bode plots should all show a phase greater than -90° and less than +90° to satisfy the KYP constraints regarding stability, see Sørensen (2013b).

3.3.3 Possible Observer Improvements

The observer can be improved by augmenting a new state, which is the low-pass filtered innovation $\tilde{\mathbf{y}}$. The observer is then an augmented observer. The observer can be further improved by assuming the wave parameters to be unknown and slowly varying. An adaptive observer can be designed which estimates the varying sea state. The observer can also be designed to count for extreme sea conditions by removing the wave estimator. Hybrid control could be used to design a system which operates optimally for a range of different sea states.

3.4 PID Controller

The proportional-integral-derivative controller dates back to the governor design in the 1890's, and is still widely used for industrial purposes. The controller is simple by design, and tuning of the controller is based on knowlegde of signal noise and empiricism.

3.4.1 Nonlinear PID control law

In Sørensen (2011), a nonlinear horizontal PID controller for moored vessels is proposed.

$$\boldsymbol{\tau}_{PID} = -\mathbf{R}_e^T\mathbf{K}_P\mathbf{e} - \mathbf{R}_e^T\mathbf{K}_{P,3}\mathbf{f}(\mathbf{e}) - \mathbf{K}_D\tilde{\boldsymbol{\nu}} - \mathbf{R}^T(\psi)\mathbf{K}_I\mathbf{z} \tag{3.17}$$

In Equation (3.17), the parameters $\{\mathbf{K_P}, \mathbf{K_{P,3}}, \mathbf{K_D}, \mathbf{K_I}\}$ are the non-negative tuning matrices for the nonlinear PID control law. $\mathbf{e}$ is the deviation from the desired position and heading, $\mathbf{R}^T(\psi)$ is the rotation matrix defined in Chapter 2, $\tilde{\boldsymbol{\nu}}$ is the deviation from the desired speed, and $\mathbf{z}$ is the integrator states:

$$\mathbf{e} = [e_1, e_2, e_3]^T = \mathbf{R}^T(\psi_d)(\hat{\boldsymbol{\eta}} - \boldsymbol{\eta}) \tag{3.18a}$$

$$\tilde{\boldsymbol{\nu}} = \hat{\boldsymbol{\nu}} - \mathbf{R}^T(\psi_d)\dot{\boldsymbol{\eta}}_d \tag{3.18b}$$

$$\dot{\mathbf{z}} = \hat{\boldsymbol{\eta}} - \boldsymbol{\eta} \tag{3.18c}$$

$$\mathbf{R}_e = \mathbf{R}(\psi - \psi_d) \triangleq \mathbf{R}^T(\psi_d)\mathbf{R}(\psi) \tag{3.18d}$$

The parameter $\boldsymbol{\eta}_d$ is the desired setpoint for the vessel, while the second term in Equation (3.17) is a third order stiffness term. The nonlinear stiffness term ensures aggressive restoring forces for large deviations from the desired position:

$$\mathbf{f}(\mathbf{e}) = [e_1^3, e_2^3, e_3^3]^T \tag{3.19}$$

3.5 Wind Feed Forward

The forces produced by wind could be predicted and counteracted by a feed-forward wind control law. The law is based on measured wind velocities from windsensors and a reliable wind force model. For semisubmersibles, the wind force constants for huge floating ocean structures, as proposed by Kitamura, Sato, Shimada, and Mikami (1997), can be used to estimate feed-forward wind forces, $\hat{\boldsymbol{\tau}}_{wind}$.

$$\boldsymbol{\tau}_{wff} = -\mathbf{K}_{wind}\hat{\boldsymbol{\tau}}_{wind} \tag{3.20}$$

In Equation (3.20), $\mathbf{K}_{wind}$ is the feed-forward gain matrix. In this Master's Thesis, it is further assumed that the wind-forces are counteracted by the feed-forward wind control law. Wind forces are therefore neglected in the simulations.

3.6 Roll and Pitch Damping

A horizontal controller can be expanded to include roll and pitch damping (RPD). This control law will dampen undesired hydrodynamic coupling effects between the surge and pitch, and roll and sway degrees of freedom. A feedback loop will result in the low frequency roll and pitch angular velocities being incorporated in the surge and sway control dynamics. If a linear formulation is used, the control law for 3 DOF can be formulated

according to Strand and Sørensen (2000).

$$\boldsymbol{\tau}_{rpd}^{3} = -\mathbf{D}_{rpd}^{3} \begin{bmatrix} \hat{p} \\ \hat{q} \end{bmatrix} = - \begin{bmatrix} 0 & d_{xq} \\ d_{yp} & 0 \\ d_{\psi p} & 0 \end{bmatrix} \begin{bmatrix} \hat{p} \\ \hat{q} \end{bmatrix} \tag{3.21}$$

It can be shown that the roll and pitch damping controll law contribute to a larger total damping of the system, reducing the motions resulting from the coupling effects.

For CyberRig I, which is symmetric fore to aft, there is no hydrodynamic coupling between sway and yaw degrees of freedom. The roll and pitch damping gain for yaw can therefore be set equal to zero; $d_{\psi p} = 0$. Due to symmetry, the surge-pitch coupled dynamics and the sway-roll coupled dynamics can be studied separately. The control law for a quadratic and symmetric vessel then becomes

$$\boldsymbol{\tau}_{rpd}^{3} = -\mathbf{D}_{rpd}^{3} \begin{bmatrix} \hat{p} \\ \hat{q} \end{bmatrix} = - \begin{bmatrix} 0 & d_{xq} \\ d_{yp} & 0 \\ 0 & 0 \end{bmatrix} \begin{bmatrix} \hat{p} \\ \hat{q} \end{bmatrix}. \tag{3.22}$$

The total control law can be formulated

$$\boldsymbol{\tau}_{c}^{5} = \boldsymbol{\tau}_{wff} + \boldsymbol{\tau}_{pid}^{3} + \boldsymbol{\tau}_{wff}^{5}. \tag{3.23}$$

3.6.1 6 DOF Stability Analysis

If only the dynamics are studied, the total control laws in surge and sway can be reduced to only the linearized PD controller and the RPD controller as seen in Equation (3.24). The reduction is made possible by the assumption that the wind feedforward controller and the integral control action will take care of the wind loads, the current loads and the mean drift loads resulting from second-order wave forces.

$$\tau_{\text{surge}} = -g_x x - d_u u - d_{xq} q \tag{3.24a}$$

$$\tau_{\text{sway}} = -g_y y - d_v v - d_{yp} p \tag{3.24b}$$

$$\tau_{\text{yaw}} = -g_\psi \psi - d_r r \tag{3.24c}$$

For a vessel with deeply submerged thrusters, such as CyberRig I when in operational mode, the physical interpretation is somewhat different. The thrusters will in addition to providing horizontal forces, also provide rotational forces due to the moment arm about the center of gravity (CG). The resulting impact on the rig, assuming no losses, time delays

or thruster dynamics, can be seen in Equation (3.29).

$$\tau_{\text{surge}} = -g_x x - d_u u - d_{xq} q \tag{3.25a}$$
$$\tau_{\text{sway}} = -g_y y - d_v v - d_{yp} p \tag{3.25b}$$
$$\tau_{\text{roll}} = l_z \cdot d_{yp} p \tag{3.25c}$$
$$\tau_{\text{pitch}} = -l_z \cdot d_{xq} q \tag{3.25d}$$
$$\tau_{\text{yaw}} = -g_\psi \psi - d_r r \tag{3.25e}$$

The moment arm l_z is positively defined, that is $l_z = |l_z|$, and represents the physical distance from the centre of gravity to the vertical position of the thrusters. The differing sign for the moment in roll encountered in Equation (3.25c), can be explained by the definition of rotational directions in Figure 3.3. A positive thruster force in y-direction will lead to a negatively defined moment in roll.

A stability analysis based on the dynamic equations in surge-pitch, and sway-roll has been performed in Strand and Sørensen (2000) and in Strand (1999). Unfortunately, it turned out the analysis include a sign error which makes the stability proof invalid. The stability analysis did also make the mistake of not taking the resulting thruster moments in roll and pitch into account.

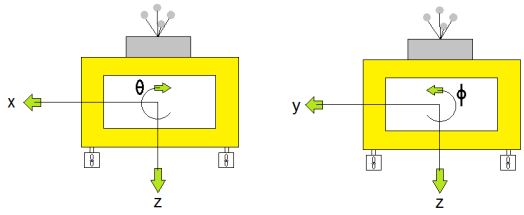

Figure 3.3: Outline of NED coordinate system with associated angular directions.

For the further analysis also, no thruster dynamics are considered, nor is the time delay in estimated signals produced by the observer. By assuming that no thruster force losses are present, the resulting forces and moments can be calculated:

$$\boldsymbol{\tau}^5_{rpd} = -\mathbf{D}^5_{rpd}\boldsymbol{\nu} = -\begin{bmatrix} 0 & 0 & 0 & 0 & d_{xq} & 0 \\ 0 & 0 & 0 & d_{yp} & 0 & 0 \\ 0 & 0 & 0 & 0 & 0 & 0 \\ 0 & 0 & 0 & -l_z \cdot d_{yp} & 0 & 0 \\ 0 & 0 & 0 & 0 & l_z \cdot d_{xq} & 0 \\ 0 & 0 & 0 & 0 & 0 & 0 \end{bmatrix} \boldsymbol{\nu} \tag{3.26}$$

The resulting 5 DOF roll and pitch damping matrix $\mathbf{D}^5_{rpd}$ needs to be positive semidefinite

for the system to be stable. The eigenvalues of the 6 DOF matrix $\mathbf{D}_{rpd}^{5}$ are stated in Equation (3.27). It can be seen that the roll-to-sway gain d_{yp} needs to be less than or equal to zero to attain a positive semi-definite roll and pitch damping matrix.

$$\boldsymbol{\lambda}_{rpd} = [\lambda_1, \cdots, \lambda_6]^T = \begin{bmatrix} 0, & 0, & 0, & -l_z \cdot d_{yp}, & l_z \cdot d_{xq}, & 0 \end{bmatrix}^T \tag{3.27}$$

If the forces and moments resulting from the linearized PD law are also taken into account, the total resulting control output matrix will consist of a damping term, and a proportional term:

$$\boldsymbol{\tau}_c^5 = \boldsymbol{\tau}_{c,D}^5 + \boldsymbol{\tau}_{c,P}^5 \tag{3.28a}$$

$$\boldsymbol{\tau}_{c,D}^5 = -\begin{bmatrix} d_{xu} & 0 & 0 & 0 & d_{xq} & 0 \\ 0 & d_{yv} & 0 & d_{yp} & 0 & 0 \\ 0 & 0 & 0 & 0 & 0 & 0 \\ 0 & -l_z \cdot d_{\phi v} & 0 & -l_z \cdot d_{yp} & 0 & 0 \\ l_z \cdot d_{\theta u} & 0 & 0 & 0 & l_z \cdot d_{xq} & 0 \\ 0 & 0 & 0 & 0 & 0 & 0 \end{bmatrix} \boldsymbol{\nu} \tag{3.28b}$$

$$\boldsymbol{\tau}_{c,P}^5 = -\begin{bmatrix} g_x & 0 & 0 & 0 & 0 & 0 \\ 0 & g_y & 0 & 0 & 0 & 0 \\ 0 & 0 & 0 & 0 & 0 & 0 \\ 0 & -l_z \cdot g_y & 0 & 0 & 0 & 0 \\ l_z \cdot g_x & 0 & 0 & 0 & 0 & 0 \\ 0 & 0 & 0 & 0 & 0 & 0 \end{bmatrix} \boldsymbol{\eta} \tag{3.28c}$$

The simplified control plant model, as defined in Section 2.4.8, can be stated

$$\dot{\boldsymbol{\eta}} = \mathbf{J}(\boldsymbol{\Theta})\boldsymbol{\nu} \tag{3.29a}$$

$$\mathbf{M}\dot{\boldsymbol{\nu}} + \mathbf{D}\boldsymbol{\nu} + \mathbf{G}\boldsymbol{\eta} = \boldsymbol{\tau}_c^5 + \boldsymbol{\tau}_{\text{moor}}, \tag{3.29b}$$

$$\boldsymbol{\tau}_c^5 = \boldsymbol{\tau}_{pd}^3 + \boldsymbol{\tau}_{\text{rpd}}^5 \tag{3.29c}$$

$$= -\mathbf{K}_P\boldsymbol{\eta} - \mathbf{K}_D\boldsymbol{\nu} - \mathbf{D}_{rpd}^5\boldsymbol{\nu}, \tag{3.29d}$$

$$\boldsymbol{\tau}_{\text{moor}} = -\mathbf{J}^T(\psi)\mathbf{G}_{mo}\boldsymbol{\eta} - \mathbf{D}_{mo}\boldsymbol{\nu}. \tag{3.29e}$$

$$\mathbf{y} = \boldsymbol{\eta} \tag{3.29f}$$

Put together, Equations (3.29b) to (3.29e) yield

$$\mathbf{M}\dot{\boldsymbol{\nu}} + \overbrace{\left(\mathbf{D} + \mathbf{K}_D + \mathbf{D}_{rpd}^5 + \mathbf{D}_{mo}\right)}^{\mathbf{D}_{total}}\boldsymbol{\nu} + \overbrace{\left(\mathbf{G} + \mathbf{K}_P + \mathbf{J}^T(\psi)\mathbf{G}_{mo}\right)}^{\mathbf{G}_{total}}\boldsymbol{\eta} = \mathbf{0}. \tag{3.30}$$

The controller analysis is performed by studying the total dynamics. Since the system is nonlinear due to the rotation matrix, Lyapunov analysis is used. A positive definite Lyapunov function candidate (LFC) is chosen

$$V(\boldsymbol{\eta}, \boldsymbol{\nu}) = \frac{1}{2}\boldsymbol{\nu}^T \mathbf{M}\boldsymbol{\nu} + \frac{1}{2}\boldsymbol{\eta}^T \boldsymbol{\beta}\boldsymbol{\eta} \quad > 0, \quad \forall (\boldsymbol{\eta}, \boldsymbol{\nu}) \neq (\mathbf{0}, \mathbf{0}), \tag{3.31}$$

and the Lyapunov stability analysis can be performed:

$$\begin{aligned}
\dot{V}(\boldsymbol{\eta}, \boldsymbol{\nu}) &= \boldsymbol{\nu}^T \mathbf{M}\dot{\boldsymbol{\nu}} + \boldsymbol{\eta}^T \boldsymbol{\beta}\dot{\boldsymbol{\eta}} && \text{(3.32a)}\\
&= -\boldsymbol{\nu}^T \mathbf{D}_{total}\boldsymbol{\nu} - \boldsymbol{\nu}^T \mathbf{G}_{total}\boldsymbol{\eta} + \boldsymbol{\eta}^T \boldsymbol{\beta} \cdot \mathbf{J}(\boldsymbol{\Theta})\boldsymbol{\nu} && \text{(3.32b)}\\
&= -\boldsymbol{\nu}^T \mathbf{D}_{total}\boldsymbol{\nu} - \boldsymbol{\nu}^T \left[\mathbf{G}_{total} - \mathbf{J}(\boldsymbol{\Theta}) \cdot \boldsymbol{\beta}\right] \boldsymbol{\eta} && \text{(3.32c)}\\
&\approx -\boldsymbol{\nu}^T \mathbf{D}_{total}\boldsymbol{\nu} - \boldsymbol{\nu}^T \left[\mathbf{G}_{total} - \mathbf{I}_{6\times 6} \cdot \boldsymbol{\beta}\right] \boldsymbol{\eta} && \text{(3.32d)}\\
&= -\boldsymbol{\nu}^T \mathbf{D}_{total}\boldsymbol{\nu} && \text{(3.32e)}\\
&\leq -\lambda_{min}(\mathbf{D}_{total}) \cdot \boldsymbol{\nu}^T \boldsymbol{\nu} && \text{(3.32f)}\\
&= -\lambda_{min}(\mathbf{D}_{total}) \cdot \|\boldsymbol{\nu}\| \quad \leq 0 && \text{(3.32g)}
\end{aligned}$$

In Equation (3.31), the virtual matrix $\boldsymbol{\beta}$ is set to be positive definite and equal to $\mathbf{G}_{total}$. The Lyapunov function candidate is then positive definite, radially unbounded and decrescent. The derivative of the LFC is negative semi-definite. The search for a better LFC could possibly result in a negative definite $\dot{V}$.

To prove that $\boldsymbol{\nu} = \mathbf{0} \Rightarrow \boldsymbol{\eta} = \mathbf{0}$, one needs to study Equation (3.30). The equilibrium $\boldsymbol{\nu} \equiv \mathbf{0}$ implies $\dot{\boldsymbol{\nu}} \equiv \mathbf{0}$. Equation (3.30) is then reduced to

$$\mathbf{G}_{total}\boldsymbol{\eta} = \mathbf{0} \quad \Rightarrow \quad \boldsymbol{\eta} = \mathbf{0}. \tag{3.33}$$

Krazowskii-LaSalle's theorem is used to prove that the control system dynamics is globally asymptotically stable (GAS). Krazovskii-LaSalle's theorem is reproduced from Fossen (2011) with some minor changes:

Krazovskii-LaSalle's theorem (Fossen (2011), page 534)
Let $V : \mathbb{R}^n \to \mathbb{R}_+$ be a continuously differentiable positive definite function such that

$$V(\boldsymbol{\eta}, \boldsymbol{\nu}) \to \boldsymbol{\infty} \text{ as } \|(\boldsymbol{\eta}, \boldsymbol{\nu})\| \to \infty \tag{3.34}$$

$$\dot{V}(\boldsymbol{\eta}, \boldsymbol{\nu}) \leq 0, \quad \forall (\boldsymbol{\eta}, \boldsymbol{\nu}) \tag{3.35}$$

Let Ω be the set where $\dot{V}(\boldsymbol{\eta}, \boldsymbol{\nu}) = 0$, that is

$$\Omega = \{(\boldsymbol{\eta}, \boldsymbol{\nu}) \in \mathbb{R}^n | \dot{V}(\boldsymbol{\eta}, \boldsymbol{\nu}) = 0\} \tag{3.36}$$

and M be the largest invariant set in Ω. Then all solutions $(\boldsymbol{\eta}(t), \boldsymbol{\nu}(t))$ converge to M. If $M = \{\mathbf{x}_e\}$, the the equilibrium point $\mathbf{x}_e$ of Equation (3.30) *is GAS.*

In this case, $M = (\mathbf{0}, \mathbf{0})$. The equilibrium point $(\boldsymbol{\eta}, \boldsymbol{\nu}) = (\mathbf{0}, \mathbf{0})$ is now proved GAS.

Assumptions

The conclusion in Equation (3.32), which yields $V(\boldsymbol{\eta}, \boldsymbol{\nu}) > 0$ and $\dot{V}(\boldsymbol{\eta}, \boldsymbol{\nu}) \leq 0$, builds on the following assumptions:

- The total damping matrix $\mathbf{D}_{total}$ is assumed positive definite.
- The total restoring matrix $\mathbf{G}_{total}$ is assumed positive definite.
- The term $\mathbf{J}(\boldsymbol{\Theta})$ is assumed positive definite and is approximated equal to the identity matrix for small angles of rotation, as shown in Section 2.1.2.That is,

$$\mathbf{J}(\boldsymbol{\Theta}) = \mathbf{J}(\delta\boldsymbol{\Theta}) \approx \mathbf{I}_{6\times 6}. \tag{3.37}$$

The listed assumptions are verified through a study of parameters and dynamics. The total damping and restoring matrices will consist of the hydrodynamical terms (hyd), the mooring terms (mo), and the control terms (c). An outline of the form of the tota damping matrix $\mathbf{D}_{total}$ can be studied in Equation (3.38). The total restoring matrix $\mathbf{G}_{total}$ will have the same form. Both the mooring forces and the PD controller will lead to increased stationkeeping both for damping forces and restoring forces. The roll and pitch damping controller will lead to increased damping in roll and pitch.

$$\begin{bmatrix} D_{11,mo+hyd+c} & 0 & 0 & 0 & D_{15,hyd+c} & 0 \\ 0 & D_{22,mo+hyd+c} & 0 & D_{24,hyd+c} & 0 & 0 \\ 0 & 0 & D_{33,hyd} & 0 & 0 & 0 \\ 0 & D_{42,hyd+c} & 0 & D_{44,hyd+c} & 0 & 0 \\ D_{51,hyd+c} & 0 & 0 & 0 & D_{55,hyd+c} & 0 \\ 0 & 0 & 0 & 0 & 0 & D_{66,mo+hyd} \end{bmatrix} \tag{3.38}$$

The rotation angles can be assumed small because semi-submersibles are realtively stable in roll and pitch, and the yaw angle is restricted by spread mooring.

Regarding the dynamics, the following assumptions are made:

- Perfect thruster dynamics, actual thrust is equal to commanded thrust at all times
- No time delays in any part of the system
- Correct LF estimates of the rotational angular velocities p and q at all times

These assumptions will not hold in the practical control system, and the actual performance of the control system can only be verified through simulations and model tests. The simulation and model test results are presented in Chapter 4.

Neglected Thruster Effects

When assuming that Equation (3.26) is valid, the following thruster effects and losses are not considered:

- Thruster to thruster interaction, i.e. one thruster operating in the wake of another thruster.
- Thruster to hull effects, i.e. the Coanda effect or not optimal incoming water on the operational zone of the thruster.
- Unsteady inflow due to vessel motion.
- Thruster dynamics are neglected, which is a fair assumption when controlling LF processes.

3.6.2 Acceleration Feedback

There exist several control concepts which can be used to improve an already well functioning control law. Extending the roll pitch damping controller by adding an acceleration feedback term has been tested by Xu et al. (2013). That is,

$$\boldsymbol{\tau}_{rp} = -\mathbf{D}_{rpd} \begin{bmatrix} p \\ q \end{bmatrix} - \mathbf{K}_{rp,acc} \begin{bmatrix} \dot{p} \\ \dot{q} \end{bmatrix}, \tag{3.39}$$

where $\mathbf{K}_{rp,acc} \in \mathbb{R}^{3\times 2}$ is the acceleration feedback gain matrix. Despite the good intentions, the study performed by Xu et al. (2013) resulted in better damping in roll and pitch, but at the same time stationkeeping accuracy was clearly reduced.

3.7 Optimal Setpoint Chasing

A regularly used method in stationkeeping today, is keeping the vessel within a small region around a desired reference point. This reference point can be set in a range of different ways. By default, this point is set to the point of operation, e.g. above the wellhead. Waves, wind and current will try and deviate the vessel body center away from this point. These forces can be both slowly and rapidly varying. A simple controller, e.g. PID, can ensure stationkeeping around a given setpoint.

The mooring system is installed in such a way that the vessel is in equilibrium in the operating point for a condition of zero external forces. The mooring line forces will in addition vary as external forces act on the vessel. One of the most critical failure modes is the loss of one or more mooring lines. To prevent this, it is recommended to ensure

that the mooring line forces are well below the critical tension level. Tension control can be implemented by setting a desired setpoint to a point were all mooring line forces are below the critical level. This method is called optimal setpoint chasing based on a structural reliability criterion.

The idea of using structural reliability in marine control applications was first implemented based on riser angles by Leira et al. (2002). It was discovered that the riser angles could be used to estimate the position of the vessel, so no extra position references were needed. Later, Nguyen and Sørensen (2009a) studied the use of setpoint chasing based on structural reliability for PM. To ensure structural reliability, the statistics of mooring line tension extremes are analyzed.

3.7.1 Extreme Values

The structural reliability index is based on a statistical analysis of mooring line tensions in the current vessel and mooring setup. In Fang et al. (2013), such an analysis has been performed for an FPSO, resulting in the Weibull distribution giving best fit for the local maxima of mooring tension. The cumulative density function (CDF) for the Weibull distribution is defined

$$F(y) = 1 - \exp\left[-\left(\frac{y}{\theta_w}\right)^{\beta_e}\right], \tag{3.40}$$

where θ_w is the scale parameter, and β_w is the shape parameter. For the statistics of extreme values, a Gumbel distribution is normally used. The CDF for the Gumbel distribution is defined equal to

$$F(Y) = \exp\left[-\exp\left[-\alpha(Y-u)\right]\right]. \tag{3.41}$$

The relation between the Weibull and Gumbel distribution parameters is given by

$$u = \theta_w (\ln N)^{\frac{1}{\beta_w}}, \tag{3.42a}$$

$$\alpha = \frac{\beta_w}{\theta_w} (\ln N)^{\frac{\beta_w - 1}{\beta_w}}, \tag{3.42b}$$

where N is the number of local maxima. The expected extreme value can be calculated

$$Y_{ex} = \theta_w \left((\ln N)^{\frac{1}{\beta_w}} + \frac{\gamma}{\beta_w (\ln N)^{\frac{\beta_w - 1}{\beta_w}}} \right). \tag{3.43}$$

An alternative way of calculating the expected extreme value is used in Leira et al. (2004), where a gust factor k is used.

$$Y_{ex} = k\sigma \tag{3.44}$$

In Equation (3.44), σ is the standard deviation of basic data series of the mooring line tensions. The gust factor is normally in the range $k = 3 - 4$.

3.7.2 Setpoint Chasing

The mooring line tension for each mooring line, when considering only the static and linear behaviour of mooring lines, can be expressed as in Equation (3.45). T_{0i} is the working point for each mooring line, c_i is the incremental stiffness tension at the present instantaneous working point, and β_{i0} is the instantaneous mooring force angle, while β is the course angle.

$$T_i = T_{0i} + c_i \Delta h \tag{3.45a}$$
$$= T_{0i} + c_i \Delta r \cos(90^\circ - \beta - \beta_{i0}) \tag{3.45b}$$
$$= T_{0i} + c_i \Delta r \sin(\beta - \beta_{i0}) \tag{3.45c}$$

A set-point chasing algorithm was introduced in Fang and Blanke (2011) which produces an optimal position increment, Δr, and an optimal direction of the position increment, β.

$$\Delta r = \frac{K_{11} \sin\beta + K_{12} \cos\beta}{K_{21} \sin^2\beta + 2K_{22} \sin\beta \cos\beta + K_{23} \cos^2\beta} \tag{3.46a}$$
$$\beta = \tan^{-1}\left(\frac{K_{11}K_{23} - K_{12}K_{22}}{K_{21}K_{12} - K_{11}K_{22}}\right) \tag{3.46b}$$

The constants $K_{ij},$ for $i = 1, 2, j = 1, 2, 3$, depend on the mooring line geometry and are evaluated in Equation (3.49).

3.7.3 Reliability Criterion

To ensure mooring line integrity, the mooring line failure load is quantified. This is solved by introducing a reliability index for each mooring line. In Berntsen, Aamo, and Leira (2006), the reliability index is defined

$$\delta_i(t) = \frac{T_{ci} - T_{exi}}{\sigma_{ci}}, \quad i = 1, \ldots, N, \tag{3.47}$$

where T_{ci} is the mean critical breaking strength of mooring line i, T_{exi} is the extreme value of the mooring line tension, and σ_{ci} is the standard deviation of the critical strength. The extreme mooring line tension kan be calculated according to $T_{exi} = T_i + k_i\sigma_i$, where k_i is the gust factor for mooring line i from Equation (3.44). In the reliability index, the standard deviation of dynamic tension should have been included. Because of this, the reliability criterion δ_i is defined larger than in reality.

3.7.4 Optimal Setpoint Chasing

An object function covering all mooring lines is presented in Fang et al. (2013).

$$L(\delta_{m1}, \delta_{m2}, \ldots, \delta_{mN}) = \sum_{i=1}^{N} \alpha_i \delta_{mi}^2 \tag{3.48a}$$

$$= \sum_{i=1}^{N} \alpha_i (\delta_{ci}^2 - \delta_i^2) \tag{3.48b}$$

Solving the partial derivative of Equation (3.48) with respect to the optimal increment Δr of the vessel position, and setting the optimal position increment and the direction of this increment equal to zero, yields the minimum value of the object function. This gives the correct gains to be inserted into Equation (3.46):

$$K_{11} = \sum_{i=1}^{N-1} \frac{\alpha_i c_i}{\sigma_{ci}} \left(\delta_{ci} - \frac{T_{ci} - T_{exi}}{\sigma_{ci}} \right) \cos \beta_{i0} + \frac{\alpha_N c_N}{\sigma_{cN}} \left(\frac{\delta_{cN} - T_{cN} - T_{exN}}{\sigma_{cN}} \right) \cos \beta_{N0} \tag{3.49a}$$

$$K_{12} = \sum_{i=1}^{N-1} \frac{\alpha_i c_i}{\sigma_{ci}} \left(\delta_{ci} - \frac{T_{ci} - T_{exi}}{\sigma_{ci}} \right) \sin \beta_{i0} + \frac{\alpha_N c_N}{\sigma_{cN}} \left(\frac{\delta_{cN} - T_{cN} - T_{exN}}{\sigma_{cN}} \right) \sin \beta_{N0} \tag{3.49b}$$

$$K_{21} = \sum_{i=1}^{N} \frac{\alpha_i c_i^2}{\sigma_{ci}^2} \cos^2 \beta_{i0} \tag{3.49c}$$

$$K_{22} = \sum_{i=1}^{N-1} \frac{\alpha_i c_i^2}{\sigma_{ci}^2} \sin \beta_{i0} \cos \beta_{i0} + \frac{\alpha_N c_N}{\sigma_{cN}} \sin^2 \beta_{N0} \tag{3.49d}$$

$$K_{23} = \sum_{i=1}^{N} \frac{\alpha_i c_i^2}{\sigma_{ci}^2} \sin^2 \beta_{i0} \tag{3.49e}$$

The updated vessel position and heading setpoint can be calculated

$$\boldsymbol{\eta} = \boldsymbol{\eta}_0 + \Delta r [\cos \beta, \sin \beta, 0]^T. \tag{3.50}$$

The set-point can be further developed to include a yaw angle set-point, meaning yaw dynamics in the spread moored system is taken into account.

3.8 Reference Model

To produce a smooth transition from the initial position to the set-point, a third order reference model is introduced, (Sørensen, 2013b).

$$\dot{\boldsymbol{\eta}}_d = \mathbf{v}_d \tag{3.51a}$$

$$\dot{\mathbf{v}}_d = -\boldsymbol{\Gamma}\boldsymbol{\eta}_d - \boldsymbol{\Omega}\mathbf{v}_d + \boldsymbol{\Gamma}\mathbf{x}_{ref} \tag{3.51b}$$

$$\dot{\mathbf{x}}_{ref} = -\mathbf{A}_f\mathbf{x}_{ref} + \mathbf{A}_f\boldsymbol{\eta}_r \tag{3.51c}$$

In Equation (3.51), $\boldsymbol{\eta}_d$ and $\mathbf{v}_d$ are the desired position and velocity in the Earth-fixed frame, respectively. $\mathbf{x}_{ref}$ is the filtered reference coordinates, and $\boldsymbol{\eta}_r$ is the new reference coordinates. The reference coordinates may be given by the setpoint chasing algorithm in Equation (3.50). The reference model is tuned through the parameters

$$\boldsymbol{\Omega} = diag[2\zeta_i\omega_i] \quad \in R^{3\times 3} > 0, \text{ for } i = 1, 2, 3, \tag{3.52a}$$

$$\boldsymbol{\Gamma} = diag[\omega_i^2] \quad \in R^{3\times 3} > 0, \text{ for } i = 1, 2, 3, \tag{3.52b}$$

$$\mathbf{A}_f = diag[1/t_i] \quad \in R^{3\times 3} > 0, \text{ for } i = 1, 2, 3, \tag{3.52c}$$

where $\boldsymbol{\Omega}$ is the diagonal damping matrix, $\boldsymbol{\Gamma}$ is the diagonal stiffness matrix, and $\mathbf{A}_f$ is the diagonal set-point filter gain matrix.

3.9 Backstepping Control Law

In Berntsen, Aamo, and Leira (2006), a feedback controller is developed using backstepping techniques. The control objective is to keep the vessel in place by ensuring mooring line integrity. The control objective is accomplished by the control law and the set-point chasing algorithm working toghether. Ensuring that this control objective is fullfilled will lead to the closed-loop system meeting the expectations regarding both the geometric task and the dynamic task. The geometric task in this case is to keep the vessel inside a given radius from the operating point.

3.9.1 Control Law

A control law is proposed

$$\boldsymbol{\tau} = \mathbf{M}\boldsymbol{\zeta} + \mathbf{D}\boldsymbol{\nu} + \mathbf{g}(\boldsymbol{\eta}) - \mathbf{R}^T(\psi)\mathbf{b}, \tag{3.53}$$

and proved GES in the article by Berntsen et al. (2006). For the control law to be GES, the control law variable $\boldsymbol{\zeta}$ is given as a function of several variables, including mooring line

parameters.

3.9.2 Stability Analysis

The control law ensures stability for the closed loop system. It should be noted that the proof submitted in the paper Berntsen et al. (2006) does not make sense if $\delta_j > \delta_s$ in open loop. To solve this, the control law can be alterated to have an active region and one inactive region defined by

$$\bar{\boldsymbol{\tau}} = \mathbf{f}(\delta_j)\boldsymbol{\tau}, \tag{3.54}$$

where $\mathbf{f}(\delta_j)$ is a nonlinear ramping function operating in the range $\mathbf{f}(\delta_j) \in [0, 1]$. Using a nonlinear passive observer (NPO) as proposed by Fossen and Strand (1999), global asymptotical stability (GAS) can be proved for the total system, i.e. the NPO and the backstepping control law in closed loop. The stability property is of course based on the standalone NPO being GES by proper tuning of the observer gain matrices.

3.10 Hybrid Control

There are several ways to merge PM and hybrid control, but the search for the best solution is not yet ended. The outline for a hybrid control system can be seen in Figure 3.4. Hybrid PM was first studied in Nguyen and Sørensen (2009a). The switching logic is here based on estimation of the sea state, and switches according to a parametrical categorization based on the sea state statistics. It is believed that the same switching could also be based on the statistical state of mooring line tension.

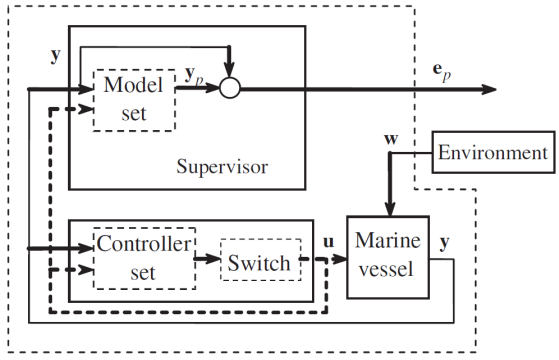

Figure 3.4: Hybrid PM controller, Sørensen (2011).

The hybrid control system consists of a set of observers with associated controllers. The switching logic decides which pair of observer and controller should be used for the current

state. In this way, the control system will work optimally for a limited number of sea states, conditions, and/or operational modes.

Chapter 4

Simulation and Model Testing

The stability of the total control system in the frequency domain has been studied in Chapter 3. The resulting performance in the time domain, however, is simulated with all subsystem dynamics. Model tests are carried out to verify the simulation results and detect errors and deficiencies in the simulation model.

4.1 Test set-up

The same mooring configuration is chosen for both the simulation model and the model test. This is done for simplicity and to avoid problems regarding interpolation. The simple mooring configuration chosen is seen in Figure 4.1. The four anchors are equally distributed along the circular configuration.

4.2 Tuning Procedure

The tuning procedure used is the same for simulations and model tests. Before the control laws can be tuned, the observer needs to produce sufficient estimates for the vessel states.

4.2.1 NPO

The NPO has fewer tuning parameters than an EKF. The tuning parameters are in addition coupled to the model parameters, since the NPO is model-based by design. The diagonal observer gain matrices are defined as in Section 3.3.2.

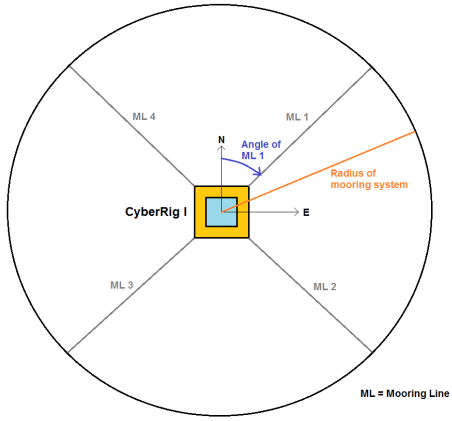

Figure 4.1: Mooring configuration used in simulations and model tests.

Firstly, only the LF dynamics is implemented and tuned through the gain matrices $\mathbf{K}_4$ and $\mathbf{K}_2$. Secondly, the wave filtering is applied with $\mathbf{K}_1(\boldsymbol{\omega_0})$. Last, the bias estimation is added, extracting the LF deviations from the estimates. The NPO gains can be studied in terms of the KYP Lemma and bode plots. The combination of $\{\mathbf{K_1}, \mathbf{K_2}, \mathbf{K_3}, \mathbf{K_4}\}$ must satisfy the KYP Lemma for every DOF and the bode plots for each DOF must show a phase shift inside the range [-90°, 90°].

4.2.2 PID

The nonlinear PID as defined in Section 3.4.1, is implemented to restore the vessel to the preset setpoint using thruster force. A PID regulator is usually tuned in the following order:

1. The $\mathbf{K}_P$ gains are tuned to restore the vessel to position within a reasonable time limit.

2. Nonlinear restoring is ensured for large deviations from setpoint by the gains in the tuning matrix $\mathbf{K}_{P,3}$.

3. The rather aggressive P-controller is damped through the $\mathbf{K}_D$ gains.

4. The steady state deviation from the given setpoint is eliminated by the $\mathbf{K}_I$ gains.

The listed tuning order is repeated till satisfying stationkeeping is accomplished.

4.2.3 RPD

The roll and pitch damping matrix gains, d_{xq} and d_{yp}, should be tuned sufficiently high as to damp LF roll and pitch motions. Simultaneously, it should not excite further roll and pitch motions. The effect on stationkeeping is used as a tuning criterion. For a symmetric semi-submersible like CyberRig I,

$$d_{xq} \approx -d_{yp}. \tag{4.1}$$

4.3 Simulation

A simulation model is made to represent the dynamics in the time domain. The simulation model consist of modelled environmental forces, the vessel dynamics, the mooring system dynamics, the observer, the control laws, and the control allocation. It should be noted that only a control plant model is used to simulate the vessel dynamics in the simulations.

4.3.1 Objectives

The objectives of performing simulations is related to the theory applied in the time domain. Simulations serve as a link between theory and the real world.

- Model the dynamics in the time domain
- Verification of performance of the different subsystems in the time domain
- Provide a basis for comparison with model tests and full scale tests

4.3.2 Overview

The simulation parameters used in the Matlab Simulink models are listed in tables in Appendix B. An overview of the Simulation model is seen in Figure 4.2.

Since a semi-submersible model block from the Simulink MSS Toolbox was used, the nonlinear damping was added on the outside of the model based on the output velocities. As for the theoretical study, current and wind is neglected.

The control law implemented in the simulations consist of the PID control law and the RPD control law:

$$\boldsymbol{\tau}_c = \boldsymbol{\tau}_{pid} + \boldsymbol{\tau}_{rpd} \tag{4.2}$$

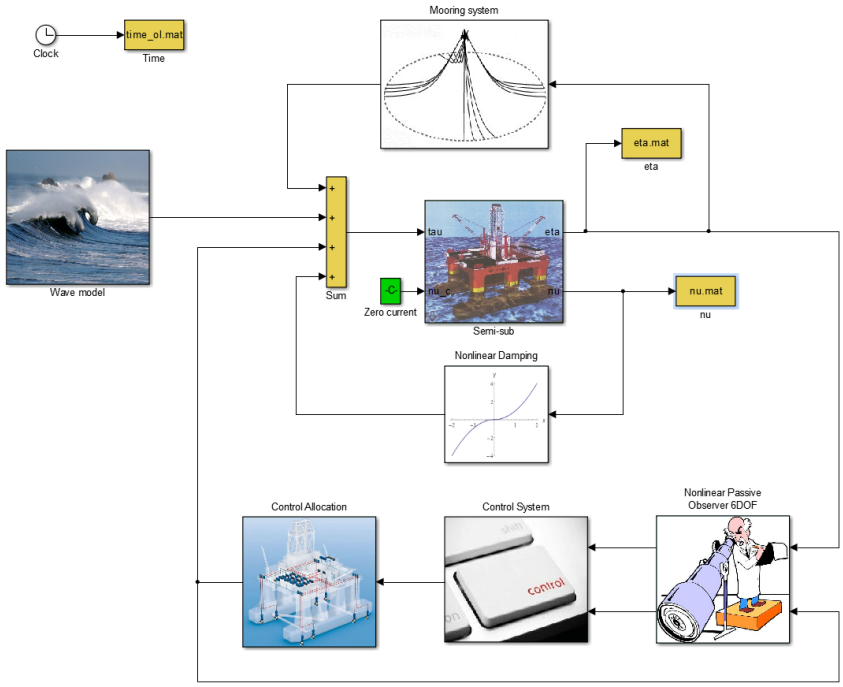

Figure 4.2: Overview of Simulink model.

4.3.3 Results

The simulations have been conducted to demonstrate the theoretical performance of the control systems, and to study how dynamics and time delays impact the control system performance. Tests with and without control input have been performed to show the improvement.

Nonlinear Passive Observer

The NPO has been tuned to give good estimates of the positions, velocities, and bias in the system in addition to filtering out the dynamics resulting from first-order wave forces. A Bode-diagram showing the frequency-domain performance of the observer in surge is seen in Figure 4.3. The observer performance for all 6 DOF in the time-domain is presented in Figure 4.4.

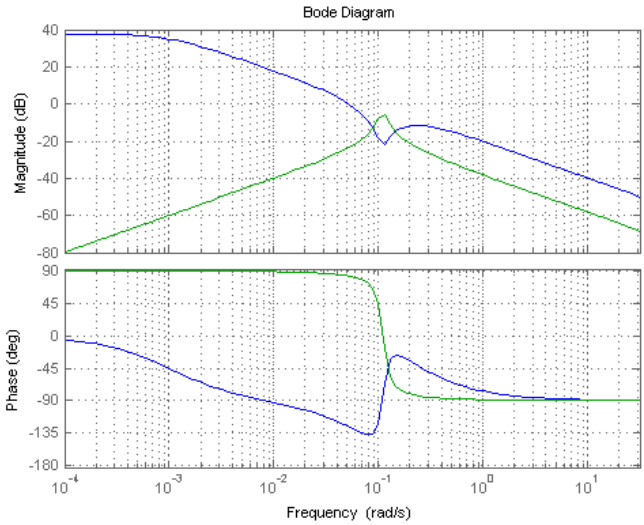

Figure 4.3: NPO bode plot for surge.

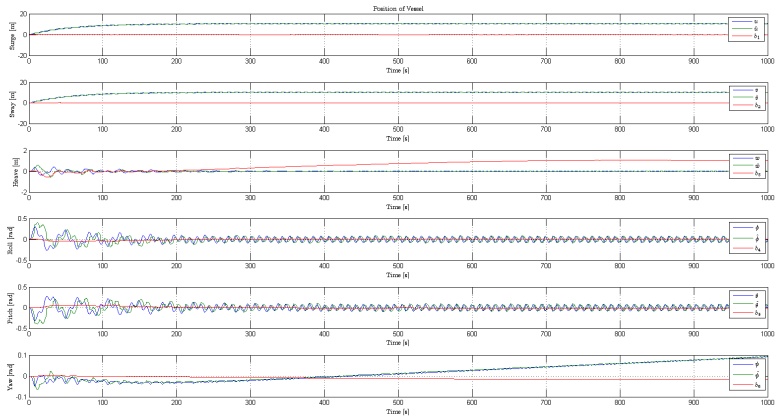

Figure 4.4: NPO performance for all 6 DOF in full scale.

PID Controller

The PID controller helps ensure stationkeeping to a greater extent than the mooring system can achieve alone, especially in harsh environments. The tuned PID gains are presented in Table 4.1.

Table 4.1: Final PID controller gains in full scale.

	K_P	K_D	K_I
Surge	10^5	10^7	10^1
Sway	10^5	10^7	10^1
Yaw	10^8	10^9	10^3

Roll and Pitch Damping Controller

The roll and pitch damping controller is implemented last. The RPD gains are tuned according to Equation (4.3) in full scale.

$$\mathbf{D}_{rpd} = \begin{bmatrix} 0 & d_{xq} \\ d_{yp} & 0 \\ 0 & 0 \end{bmatrix} = \begin{bmatrix} 0 & 10^7 \\ -10^7 & 0 \\ 0 & 0 \end{bmatrix} \tag{4.3}$$

4.4 Model Testing

To show that the theory and the simulations match the real world, model tests are conducted. The correctness of the assumptions are approved or disproved, and effects not accounted for in the mathematical modelling are detected.

4.4.1 Objectives

The objectives of performing model tests are related to the real-time control system performance. The most important are:

- Validation of model properties and parameters
- Validation of the dynamics of the model
- Verification of simulation results
- Tuning of the observer to give good estimates with short time delay
- Discovering nonlinear effects that shoul be included in the model
- Discovering probable failure modes for position mooring with roll and pitch damping

4.4.2 Test Facilities

The model tests are carried out in the Marine Cybernetics Laboratory (MCLab) at NTNU. The model tank has dimensions $L \times B \times D = 40 \times 6.45 \times 1.5$ [m], and is sufficient for control testing purposes. Recommended scale ratio is λ = 50-150. The tank is equipeed with a carriage which moves along the tank with a maximum speed of 2 [m/s], and a wave maker. The wave maker is capable of producing both regular and irregular waves with heights up to 0.25 [m] amplitude.

4.4.3 CyberRig I

For the tests of the control system performance, CyberRig I was chosen. The model semi-submersible was built by Tyssø and Aga (2006) and is equipped with eight azimuth thrusters. The model parameters and mooring configuration of CyberRig I can be found in Appendix A. The model has a mass of $m = 73$ [kg] and is quite difficult to manage practically. The horizontally anchored CyberRig I can be seen in Figure 4.5.

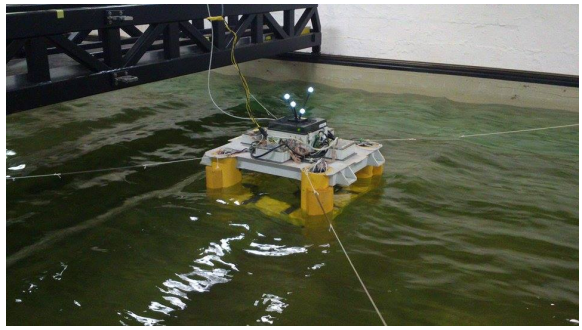

Figure 4.5: The moored CyberRig I in the MCLab.

4.4.4 Mooring System

A horizontal mooring configuration is chosen for the model tests. The horizontal configuration is simpler to install, modify and maintain during the model tests. Each mooring line is equipped with a linear spring, restoring the horizontal motions is surge, sway and yaw. The mooring configuration can be seen in Figure 4.1.

4.4.5 Hardware and Software

The data network used in the model test consists of the computer installed on CyberRig I, the control computer, and the computer receiving signals from the positioning system and calculating the position of the vessel. An overview of the data network can be seen in Figure 4.6.

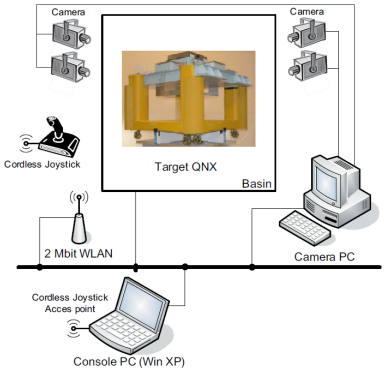

Figure 4.6: The model test data network.

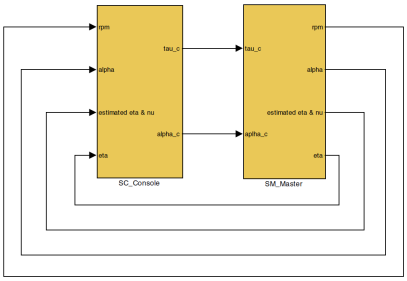

Figure 4.7: Opal RT-Lab set-up.

In addition, the control allocation system on CyberRig I has a low-level fieldbus network. The fieldbus network connects the step motors controlling the thrusters to the QNX computer installed on CyberRig I. The fieldbus network is shown in Figure A.2.

Opal RT-Lab

The software Opal RT-Lab creates the connection between the Matlab Simulink model on the console computer, the QNX computer on CyberRig I, and the data network. The master subsystem is loaded and compiled to the QNX computer installed on CyberRig I by RT-Lab. An overview of the system can be seen in Figure 4.7. The system is divided into two subsystems; the console and the master. The observer, the control allocation and the reference system signal receiver are placed in the master subsystem. The control laws, on the other hand, is placed in the console subsystem. This allows for tuning of control parameters during tests, but not for tuning of the observer gains after compilation. Since tuning of the observer proved to be a cumbersome process, the lock on observer tuning gains during tests created some extra difficulties.

Reference System

The reference system consists of 3 cameras which together produce 6 DOF position measurements

$$\mathbf{y} = \mathbf{H}\mathbf{x} = \begin{bmatrix} x & y & z & \phi & \theta & \psi \end{bmatrix}^T = \boldsymbol{\eta}. \tag{4.4}$$

Velocity or acceleration measurements are not available in the current set-up.

4.4.6 Model Test Results

Decay tests to find the linear and nonlinear damping terms for all six degrees of freedom were performed. Motion response test in regular and irregular waves were carried out. The roll and pitch damping control law was tested in irregular waves.

Decay tests

Decay tests were performed in heave, roll, and pitch before the rig was anchored. After it was moored, decay tests were carried out in 6 DOF. The results were used to determine the relative damping and natural periods. A typical decay test time series, and the method used to determine both the linear and the second-order damping parameters are presented in Figure 4.8 and Figure 4.9, respectively.

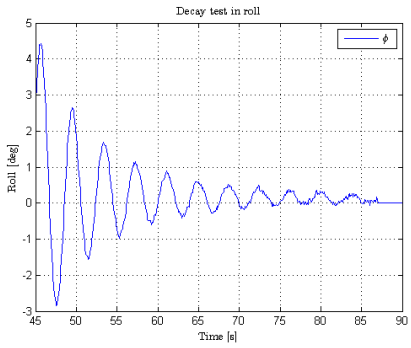

Figure 4.8: Decay test in roll.

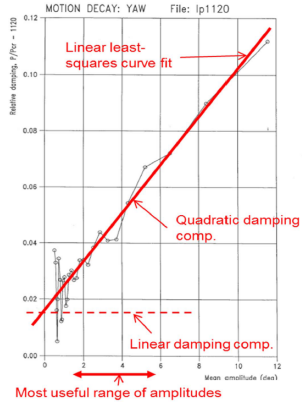

Figure 4.9: Method for determining damping, Steen (2012).

The parameters obtained during free model tests are presented in Table 4.2. For evaluation of the corresponding full scale periods, the periods in Table 4.2 are multiplied by a factor

of 10, which is in accordance with the scaling parameters presented in Equation (2.39) in Section 2.5.2.

Table 4.2: Decay test results, no mooring.

	Damping ratio [-]	Natural period [s]
Heave	0.0152	2.1994
Roll	0.0597	3.8488
Pitch	0.0659	3.8217

The natural periods obtained shows that CyberRig I has natural periods which correspond well to those of a typical full scale semi-submersible operating in the North Sea. Natural periods in heave, roll, and pitch for full scale rigs are normally in the range of 25-80 [s], according to Sørensen (2013b).

When moored, the mooring system ensures restoring in surge, sway and yaw. The linear and nonlinear damping is then estimated for all 6 DOF. Typical natural periods in surge and sway for mooring depths between $h =$ 100-500 [m], are 70-200 [s] according to Sørensen (2013b).

Table 4.3: Decay test results for spread moored model vessel.

	ξ_1 [-]	ξ_2 [-]	T_0 [s]
Surge	0.0649	0.3347	16.6436
Sway	-	-	15.7633
Heave	-	-	3.5795
Roll	0.0348	0.3582	3.4970
Pitch	0.0319	0.5513	3.5859
Yaw	0.0123	1.0471	13.9242

In Table 4.3, ξ_1 represent the linear relative damping ratio, while ξ_2 represent the second order relative damping ratio. Using these constants, linear and second order damping terms for CyberRig I can be calculated. The damping ratios for sway and heave were not calculated due to bad time series results, but it is assumed that the damping ratios in sway can be estimated nearly equal to the damping ratios in sway. The damping terms in heave are not considered important since heave is decoupled from the other DOFs and will not affect the control system performance.

The measured natural periods of the moored model vessel in Table 4.3 are in consistence with the theoretical eigenperiods of full size moored semi-submersibles. The undamped eigenperiods T_0 for the model are scaled up to full size by a factor equal to $\sqrt{\lambda} = 10$. This is in accordance with the scaling laws presented in Section 2.5.2.

Wave tests

The control system of the model semi-submersible is tested in irregular waves. The irregular waves are produced using the JONSWAP spectrum with $\omega_0 = 0.9$ [s^{-1}], $H_S = 0.06$ [m], and $\gamma = 3.3$. The JONSWAP spectrum is defined in Section 2.2.1. To be able to evaluate the performance of the control system, the model is tested in waves with no control input at first. The response spectra for surge and pitch are plotted in Figure 4.10 and Figure 4.11, respectively.

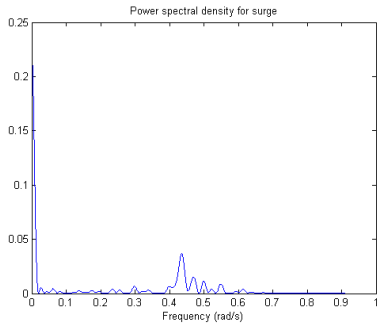

Figure 4.10: Surge response spectrum.

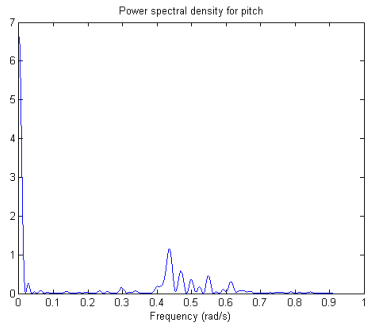

Figure 4.11: Pitch response spectrum.

The time domain results of the performance with and without roll and pitch damping control can be seen in Figure 4.12. Statistics were calculated from the timeseries presented, and are listed in Table 4.4.

Table 4.4: Controller performance in model test, $\lambda = 100$.

Parameter	Symbol	No control	RPD control	Unit
Surge mean	$\bar{x}$	0.0469	0.0010	[m]
Surge std. dev.	σ_x	0.0475	0.0101	[m]
Pitch mean	$\bar{\theta}$	0.2594	-0.0308	[deg]
Pitch std. dev.	σ_θ	0.6503	0.0575	[deg]

In Table 4.4 the statistics imply that both the mean and the standard deviation of both surge and pitch decreases under influence from the roll and pitch control law. In Figure 4.12, it can also be seen that the amplitudes are generally higher, and the low-frequent motion dominates over the wave-frequency motions under influence from the RPD controller. It should be mentioned that the test series with control input are relatively short due to problems with the model semi-submersible.

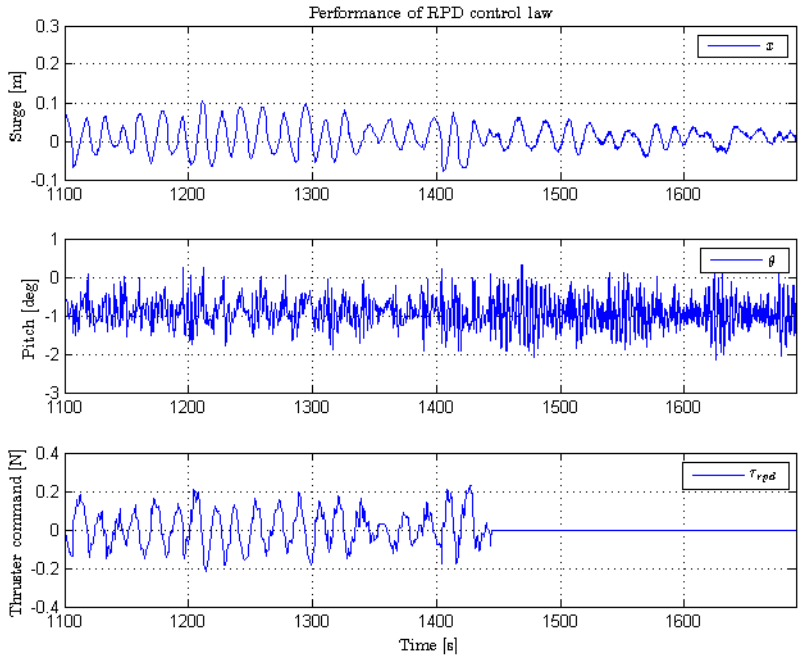

Figure 4.12: Resulting roll and pitch motions with and without control input.

Steady List Angle

The model semi-submersible was, in addition to irregular waves, also tested for regular head waves. It was observed that the rig experienced a large steady roll angle after some time, of about 10-15 [deg]. This phenomena is related to the work done by Voogt et al. (2002).

Chapter 5

Discussion

Low frequency nonlinear dynamics dominate for a moored semi-submersible in harsh weather. The dynamics of such a system and how to damp and control it, has been regarded and discussed.

5.1 Position Mooring

Several methods for position mooring are studied and found both stable, reliable and robust. The stability of the methods has been reviewed in terms on linear and nonlinear stability analyses. Reliability is ensured through a structural reliability criterion based on mooring tension statistics.

Making the system more reliable and robust requires a more complex and model-based approach. Examples of such methods and functions are the structural reliability-based setpoint chasing algorithm, and the structural reliability-based nonlinear control law derived through backstepping techniques.

The setpoint chasing algorithm will give an input to an additional stationkeeping controller, e.g. a PID controller. The algorithm ensures reliability in the manner of decreased probability of failure, but stability and robustness may only be achieved by the chosen stationkeeping control law. A controller suitable for the task could be a nonlinear PID controller. The system could be further utilized by adding a RPD controller.

The backstepping controller based on a structural reliability criterion is proved GAS in combination with a NPO. That is, a control system consisting of a backstepping controller combined with a NPO is a stable and robust system. The structural reliability criterion

contributes to making the controller reliable in manner of decreasing the probability of mooring line loss and drift off.

However, these controllers will only provide sufficient performance for a given range of parameters and conditions. The NPO, for instance, is not able to give optimal estimates for both calm and harsh environments due to the wave filtering dynamics. The observer is designed so as to be tuned optimal for one specific sea state.

Hybrid control systems are assumed to be the next step in terms of complexity and robustness. The hybrid control system consists of a set of controllers with related observers optimized for different sea states. The hybrid system toggle between the different observer and controller pairs by a custom switching logic. The switching logic is based on an estimation of the current state of the system, e.g. the sea state. For position mooring systems, one of the controllers could even consist of none control input at all, being switched on for calm seas. Then, the passive mooring system would ensure stationkeeping with no additional help. For harsh weather, additional damping and control laws based on structural reliability could be switched on. The switching logic may be based on either the sea state estimation or the mooring line load state.

5.2 Special Focus

One of the main contributions in this Master's Thesis is the theoretical study of the stability of the roll and pitch damping law in Section 3.6. It was discovered that the theoretical stability proof in Strand and Sørensen (2000) includes a sign error. Unfortunately, this sign error leaves the proof invalid. The same error is also transferred to Strand (1999). A Lyapunov stability analysis is conducted in its place, using the Krazovskii-LaSalle theorem for autonomous systems. The stability analysis proved the total system, including the linearized PD and the RPD control law, to be globally asymptotically stable. The reference model give a smooth transition to the desired setpoint.

The faults detected in Strand and Sørensen (2000) may be the reason why the simulations in Xu et al. (2013) did not work out quite as expected. Both of the papers clearly states that the RPD controller gains should be strictly positive. As the stability analysis in Section 3.6 clearly states, the off-diagonal controller gains should have signs reflecting the coupling between the surge-pitch and sway-roll.

Although the nonlinear passive observer has proven to produce good estimates in full scale simulations, difficulties arose as the nonlinear passive observer was implemented on the model scale semi-submersible. Only position measurements are available from the reference system, and wave-filtered estimates for roll and pitch angular velocities are needed for the roll and pitch damping control law.

There are several possible reasons for the bad observer performance. One of them is

short model vessel eigenperiods, which, due to the scaling ratio, is 1/10 of the full scale eigenperiods. For roll and pitch, the model scale eigenperiods are equal to 3.5 [s] for roll and 3.6 [s] for pitch. Theoretically, the computation time in model scale should also be scaled by a factor of 1/10. The computers used in the closed-loop model tests are at least 8 years old, and relatively slow. In the model tests, the phase shift between the actual angular velocity and the actual output from the thrusters soon reached -90°. It is a known fact in control theory that phase shifts below -90° or above +90° lead to bad control system performance. Direct angular velocity measurements could be obtained by installation and implementation of a gyroscope. A low pass filter could be implemented and tuned to provide the roll and pitch damping controller with LF angular velocity estimates.

Another source of error could be the solver method chosen in Simulink. The solver methods work differently for derivation, integration and other closed-loop calculations.

Since the NPO is model based, wrong model parameters could impact the performance of the observer. The properties of CyberRig I has changed due to structural upgrades. For instance, the columns' cross-sectional area have been expanded, a frame under the platform deck is removed, and the original ballast system has been replaced by a new one. The changes the parameters, e.g. the mass of the model semi-submersible has increased from 55 [kg] in Tyssø and Aga (2006), to 73 [kg] today.

5.3 Special Phenomena

The model semi-submersible was tested for regular head waves with no control input. It was observed that the rig experienced a large steady roll angle after some time. This phenomena was first studied in Numata, Michel, and McClure (1975), and has been observed and studied in model laboratories since then. In Voogt, Soles, and Dijk (2002), the steady roll angle for regular waves, with variable draught and initial stability, is adressed. The steady list is a result of vertical wave drift forces which increases as the pontoon approaches the sea surface. The phenomena of steady list can be reduced by increasing the cross sectional area of the stability columns or by increasing the operational draught. The phenomena will probably only occur in model tanks and basins where strictly regular waves can be obtained. This is because the vertical wave drift forces are constant only for regular waves, and the waves in the North Sea are typically irregular.

5.4 CyberRig I

In Section 4.4.6, the eigenperiods for CyberRig I in heave, roll and pitch are found to be correct in proportional to the eigenperiods of typical full scale semi-submersibles. The model scale roll and pitch natural periods of oscillation are equal to 3.5 [s] for roll and

3.6 [s] for pitch. Normal natural periods in roll and pitch for full scale semi-submersibles ranges between 25-80 [s], and the scaling ratio for periods of oscillation is equal to $T_F = \sqrt{\lambda} \cdot T_M = 10 \cdot T_M$. The heave eigenperiod is also proved comparable to full scale results.

This implies that Cyberrig is an appropriate model for experimental testing of heave, roll, and pitch dynamics. Excessive heave oscillation is a well-known problem for semi-submersibles which is solved through structural heave damping. But if CyberRig I is to be used in further experimental tests, a few changes and upgrades needs to be implemented. Appendix E is devoted to proposals for improvement of CyberRig I.

Chapter 6

Concluding Remarks

6.1 Conclusions

The objective of this Master's Thesis has been to study the low frequency dynamics of a thruster assisted position mooring system. A selection of different approches to PM was chosen and studied. Several methods added beneficial properties to the total system. Due to the lack of published results for roll and pitch damping model tests, the combination of RPD and PID was emphasized.

It was discovered that the theoretical stability proof in Strand and Sørensen (2000) includes a sign error. Unfortunately, this sign error leaves the proof invalid. The same error is also found in Strand (1999). A Lyapunov stability analysis is conducted in its place, using the Krazovskii-LaSalle theorem for autonomous systems. The stability analysis proved the total control law, including the PD and the RPD control law, to be globally asymptotically stable.

A simulation model has been derived, based on a full-scale version of CyberRig I. This model has been implemented in Matlab Simulink. The moored rig model is under impact from environmental loads, and damped using a roll and pitch damping controller. The controlled system is stable under given conditions, but is unreliable for harsh weather or mooring line loss. For such conditions, more robust control methods are needed.

The physical model tests of RPD performance proved cumbersome. Although the nonlinear passive observer proved to produce good estimates in full scale simulations, difficulties arose as the nonlinear passive observer was implemented on the model scale semi-submersible. Only position measurements are available from the reference system. Adequate wave-filtered estimates for roll and pitch angular velocities are needed for the roll and pitch damping control. The time delay in the nonlinear passive observer resulted

in a phase shift less than 90° between the actual angular velocity and the actual thruster output. This instead lead to excited oscillations in roll and pitch in the model tests. One solution could be installing a gyroscope on CyberRig I.

6.2 Further Work

From the conclusions it is clear that robust and reliable control methods should be implemented and tested. The need for safe and reliable solutions is ever increasing with the development of more complex systems and operations. The search for the optimal PM control system continues, and hybrid PM is considered tomorrow's solution.

The proposals for further work are:

- Upgrading from a control plant model to a process plant model in the simulation model
- Implementation and testing of a setpoint chasing algorithm based on the principle of structural reliability
- Implementation and testing of a nonlinear backstepping control law based on the principle of structural reliability
- Implementation and testing of roll and pitch acceleration feedback
- Compare stability and robustness of the total control systems in 6 DOF, including observer
- Study fault monitoring and fault recovery control, and discuss features to be applied in the control system
- Merge position mooring control with hybrid control and use custom switching logic for thruster assisted position mooring
- Upgrading of the model semi-submersible CyberRig I in terms of water resistance, protection of equipment, and installation and implementation of a gyroscope
- Model scale and full scale testing of the control systems

The topic of this Master's Thesis has proven both interesting and challenging. It is hoped that this Master's Thesis will stimulate further work in the field of thruster assisted position mooring systems.

Bibliography

Aamo, O. M., Fossen, T. I., 1999. Controlling line tension in thruster assisted mooring systems. In: Control Applications, 1999. Proceedings of the 1999 IEEE International Conference on. Vol. 2. IEEE, pp. 1104–1109.

Aamo, O. M., Fossen, T. I., 2001. Finite element modelling of moored vessels. Mathematical and Computer Modelling of Dynamical Systems 7 (1), 47–75.

Berntsen, P. I. B., Aamo, O. M., Leira, B. J., 2006. Dynamic positioning of moored vessels based on structural reliability. In: Decision and Control, 2006 45th IEEE Conference on. pp. 5906–5911.

DNV, 2013. Dnv-os-301: Position mooring. DNV Offshore Standards.

Faltinsen, O. M., 1990. Sea Loads on Ships and Offshore Structures. Cambridge Ocean Technology Series. Cambridge University Press.

Fang, S., Blanke, M., 2011. Fault monitoring and fault recovery control for position moored tanker. International Journal of Applied Mathematics and Computer Science 21 (3), 467–478.

Fang, S., Leira, B. J., Blanke, M., 2013. Position mooring control based on a structural reliability criterion. Structural Safety 41 (0), 97 – 106.

Faÿ, H., 1990. Dynamic positioning systems: Principles, design and applications. Editions OPHRYS.

Fossen, T. I., 2011. Handbook of Marine Craft Hydrodynamics and Motion Control. John Wiley & Sons.

Fossen, T. I., Strand, J. P., 1999. Passive nonlinear observer design for ships using lyapunov methods: full-scale experiments with a supply vessel. Automatica 35 (1), 3 – 16.

Khalil, H. K., 2002. Nonlinear Systems. Prentice Hall.

Kitamura, F., Sato, H., Shimada, K., Mikami, T., Oct 1997. Estimation of wind force acting on huge floating ocean structures. In: OCEANS '97. MTS/IEEE Conference Proceedings. Vol. 1. pp. 197–202 vol.1.

Leira, B. J., Sørensen, A. J., Larsen, C. M., 2002. Reliability-based schemes for control of riser response and dynamic positioning of floating vessels. In: ASME 2002 21st International Conference on Offshore Mechanics and Arctic Engineering. American Society of Mechanical Engineers, pp. 441–449.

Leira, B. J., Sørensen, A. J., Larsen, C. M., 2004. A reliability-based control algorithm for dynamic positioning of floating vessels. Structural Safety 26 (1), 1 – 28.

Nguyen, D. T., Sørensen, A. J., 2009a. Setpoint chasing for thruster-assisted position mooring. Oceanic Engineering, IEEE Journal of 34 (4), 548–558.

Nguyen, D. T., Sørensen, A. J., 2009b. Switching control for thruster-assisted position mooring. Control Engineering Practice 17 (9), 985 – 994.

Nguyen, T. D., 2006. Design of hybrid marine control systems for dynamic positioning. Ph.D. thesis, National University of Singapore (NUS), Department of Civil Engineering.

Numata, E., Michel, W. H., McClure, A. C., 1975. Experimental study of stability units for semi-submersible drilling platforms. SPE-AIME Seventh Annual Offshore Conference, Houston.

Smogeli, O. N., Ruth, E., Sørensen, A. J., 2005. Experimental validation of power and torque thruster control. In: Intelligent Control, 2005. Proceedings of the 2005 IEEE International Symposium on, Mediterrean Conference on Control and Automation. pp. 1506–1511.

Steen, S., 2012. Experimental methods in marine hydrodynamics, lecture notes, ntnu.

Strand, J. P., 1999. Nonlinear position control systems design for marine vessels. Ph.D. thesis, Norwegian University of Science and Technology, Department of Engineering Cybernetics.

Strand, J. P., Sørensen, A. J., 2000. Positioning of small-waterplane-area marine constructions with roll and pitch damping. Control Engineering Practice 8 (2), 205 – 213.

Strand, J. P., Sørensen, A. J., Fossen, T. I., 1998. Design of automatic thruster assisted mooring systems for ships. Modeling, Identification and Control 19 (2), 61–75.

Sørensen, A. J., 2011. A survey of dynamic positioning control systems. Annual Reviews in Control 35 (1), 123 – 136.

Sørensen, A. J., 2013a. Advanced model-based design and testing of marine control systems, lecture notes, ntnu.

Sørensen, A. J., 2013b. Marine control systems, lecture notes, ntnu.

Sørensen, A. J., Sagatun, S. I., Fossen, T. I., 1996. Design of a dynamic positioning system using model-based control. Control Engineering Practice 4 (3), 359 – 368.

Teel, A., Sanfelice, R., Goebel, R., 2011. Hybrid control systems. In: Meyers, R. A. (Ed.), Mathematics of Complexity and Dynamical Systems. Springer New York, pp. 704–728.

Torsethaugen, K., 1996. Model for a doubly peaked wave spectrum. SINTEF report STF22 A 96204.

Triantafyllou, M., 1990. Cable mechanics with marine applications. Document prepared for instruction in the Ocean Engineering Department at the Massachusetts Institute of Technology.

Tyssø, J., Aga, A. H., 2006. Dp control system design for cyberrig i. Master's thesis, Norwegian University of Science and Technology, Department of Engineering Cybernetics.

Voogt, A. J., Soles, J. J., Dijk, R. V., 2002. Mean and low frequency roll for semi-submersible in waves. ISOPE Conference, Kitakyushu, Japan.

Xu, S., Wang, X., Wang, L., Li, J., 2013. Dynamic positioning with roll-pitch damping motion control for a semi-submersible. In: Proceedings of the twenty-third (2013) International Offshore and Polar Engineering Conference. pp. 973–978.

Appendices

Appendix A

Model Test Facilities

For model tests, CyberRig I and the MCLab with all of its equipment was offered for the purpose of model testing. CyberRig I has an associated control computer which runs the needed software for control of the semi-submersible and its thrusters.

CyberRig I

The model scale measurements of CyberRig I are listed in Table A.1. These values were adopted from Tyssø and Aga (2006).

Table A.1: CyberRig I parameters.

Parameter	Description	Value	Unit
L_{oa}	Length over all	118.5	m
B_{oa}	Breadth over all	95.4	m
L_{wl}	Length outside pontoons	84.5	m
L_{wl}	Breadth outside pontoons	84.5	m
H_c	Heigth to underside box structure	39.5	m
H_t	Heigth to upper dech	40.0	m
B_p	Pontoon breadth	39.5	m
H_p	Pontoon heigth	8.4	m
D_o	Operating draught	23.0	m

In Table A.2, volumetric parameters for CyberRig I are listed. The abbreviation CB stands for center of buoyancy.

The thrusters are allocated under CyberRig I as shown in Figure A.1.

Table A.2: Cyberrig I volumetric parameters.

Parameter	Description	Value	Unit
KB_p	Pontoon CB	4.2	cm
KB_c	Column CB	12.0	m
KB_x	Extra column CB	16.1	m
∇_p	Pontoon displacement	713.9	cm^3
∇_c	Column displacement	661.3	cm^3
∇_x	Extra column displacement	912.6	cm^3
y_c	Length to center of column	33.9	cm
y_x	Length to center of extra column	44.2	cm

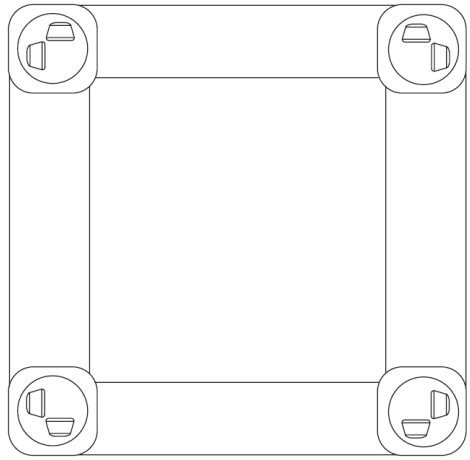

Figure A.1: The thruster configuration for CyberRig I.

The fieldbus network which connects the thrusters and the QNX computer is depicted from above in Figure A.2.

The Marine Cybernetics Laboratory

For model testing, the environment is reproduced in model scale. At the Norwegian University of Science and Technology (NTNU), control system model testing is made possible in the NTNU Marine Cybernetics Laboratory (MCLab). The facilities available is a long test tank with dimensions $L \times B \times D = 40 \times 6.45 \times 1.5$ [m]. The tank is equipeed with a carriage which moves along the tank, and a wave maker. In this Master's thesis, only the wave maker have been used.

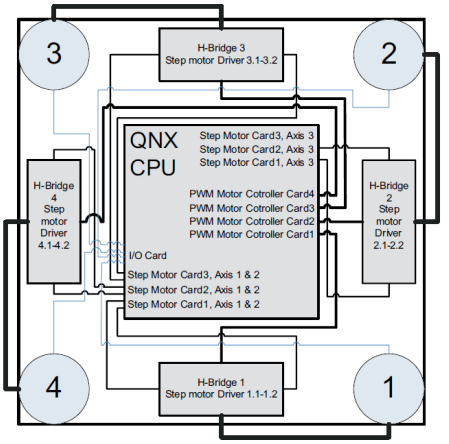

Figure A.2: The fieldbus network on CyberRig I.

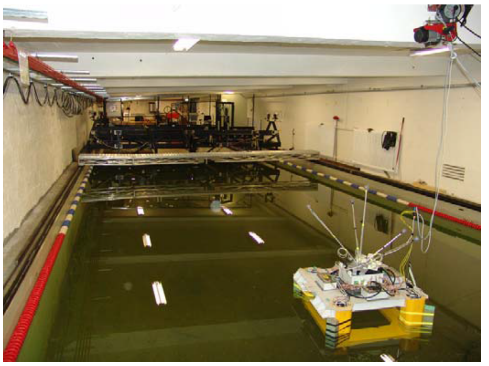

Figure A.3: Cyberrig I in MCLab.

The Wave Maker

The wave maker at the MCLab can produce both regular and irregular waves. The capacity of the wave maker is found to be $H < 0.25$ [m], $T = 0.3 - 3$ [s] for regular waves, and $H_s < 0.15$ [m], $T = 0.6 - 1.5$ [s] for irregular waves. Several wave spectrums are available for the generation of irregular waves, including JONSWAP, Pierson-Moskowitz, ITTC, etc.

Qualisys Track Manager

The tracking system in the MCLab consists of three Oqus cameras attached to the carriage, and a marker antler which is placed on top of CyberRig I. The Track Manager provide measured positions for all six degrees of freedom; three longitudinal and three rotational positions. The six states provided by the Qualisys Track Manager are the only measured states in the feedback system, as illustrated in Equation (A.1).

$$\mathbf{y} = \mathbf{H}\mathbf{x} = \begin{bmatrix} x & y & z & \phi & \theta & \psi \end{bmatrix}^T \tag{A.1}$$

Appendix B

Simulation Parameters

Environmental Parameters

The typical environmental parameters for the North Sea in Table B.1 are adopted from Sørensen (2013a). The environmental parameters used for the creation of irregular waves

Table B.1: Simulation environmental parameters.

Parameter	Description	Size	Unit
H_s	Significant wave height	$\in$[0.5,12]	m
$\bar{H}_s$	Average significant wave height	2.7	m
T_p	Peak period	$\in$ [1,18]	s
V_w	Wind speed	$\in$ [0,33.4]	ms^{-1}
$\bar{V}_w$	Average wind speed	8.4	ms^{-1}
V_c	Current velocity	$\in$ [0,1.5]	ms^{-1}

in the model tests are listed in Table

Table B.2: Model test environmental parameters.

Parameter	Description	Size	Unit
H_s	Significant wave height	0.06	m
$\bar{H}_s$	Average significant wave height	2.7	m
T_p	Peak period	1/0.8	s
V_w	Wind speed	0	ms^{-1}
$\bar{V}_w$	Average wind speed	0	ms^{-1}
V_c	Current velocity	0	ms^{-1}

Mooring System Parameters

The mooring system parameters are estimated based on Aamo and Fossen (2001) and Sørensen (2013b). The stability of the system is strongly dependent on the ratios between depth, mooring cable length, and mooring cable thickness. Some of the parameters are listed in Table B.3, the rest can be found in the Matlab files in Appendix F.

Table B.3: Simulation mooring parameters.

Parameter	Description	Value	Unit
d	Depth	200	m
L	Unstretched	300	m
R_a	Anchor distribution radius	300	m
D	Cable diameter	0.08	m

Appendix C

Simulink Diagrams

The overview of the Simulink model can be seen in Chapter 4. The subsystems spand from the mooring system in Figure C.1, to the control allocation system in Figure C.6.

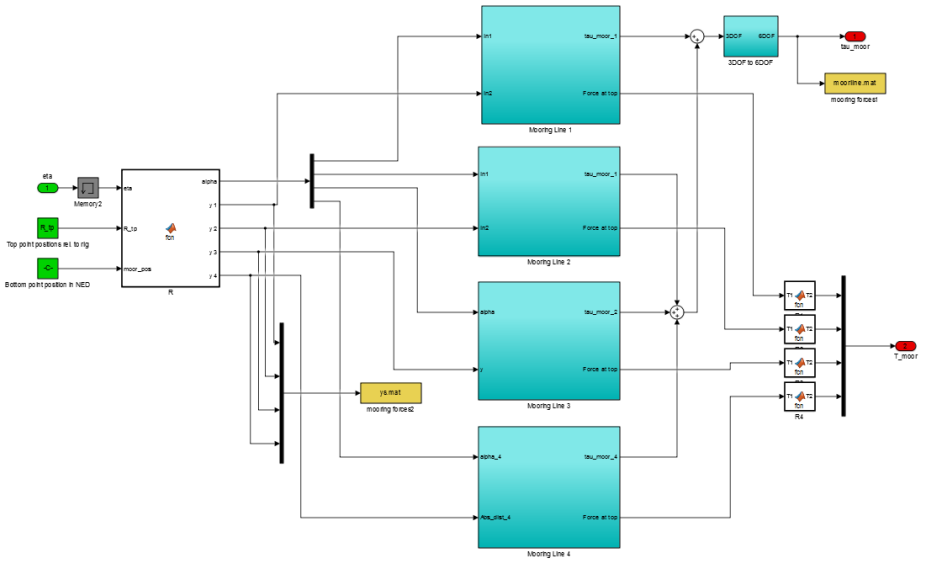

Figure C.1: The Simulink model of the mooring system.

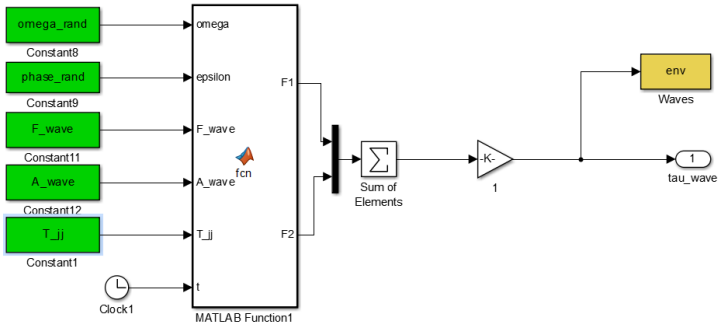

Figure C.2: The Simulink model of wave environment.

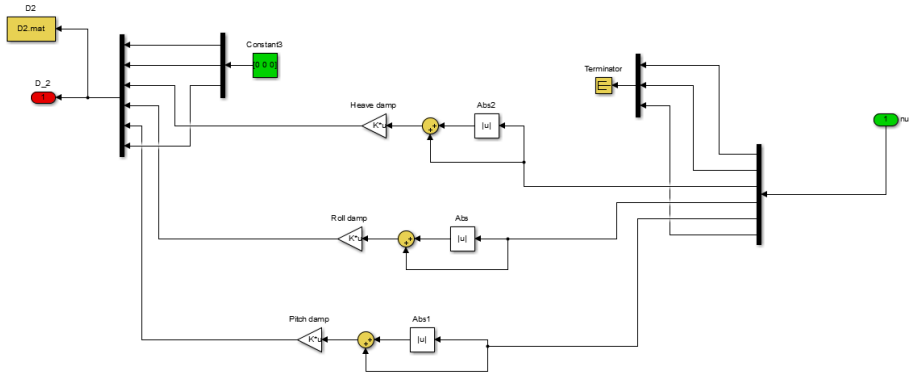

Figure C.3: The Simulink model considering the nonlinear damping.

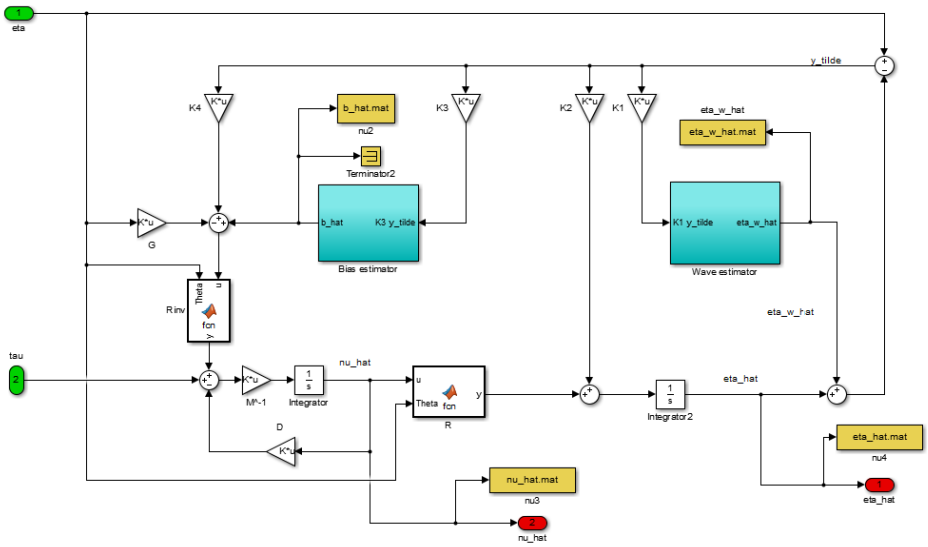

Figure C.4: The Simulink model of the NPO.

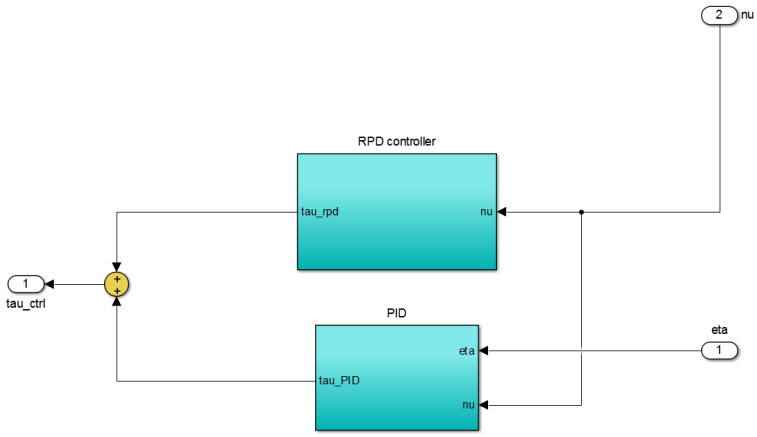

Figure C.5: The Simulink model containing the control laws.

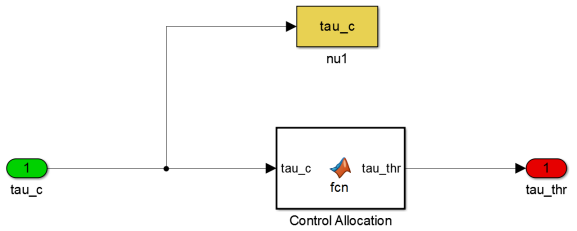

Figure C.6: The Simulink model of the control allocation system.

Appendix D

Matlab Code

The `init.m` file, which is run for the total model is displayed:

```
%% Closed Loop Simulation
clc
clear all

%% Initial values
sim_tid = 300;
eta_0 = zeros(1,6);
nr_elem = 20;
nu_c = zeros(1,6);
tau_moor = zeros(1,6);

%% Scaling parameters
rho_M = 1000;
rho_F = 1025;
lambda = 100;

% Model scale matrices for CyberRig I
MRB_M = diag([73.1,73.1,73.1,1.2360,1.2360,13.7334]);
MA_M = diag([21.6151,21.6151,70.6667,5.0898,5.0898,2.9725]);
MA_M(5,1) = 2.5743; MA_M(4,2) = -2.5743; MA_M(1,5) = 2.5461; MA_M(2,4) = -2.5461;
D_M = diag([16.1482,16.1481,0.0319,0,0.0552,3.2798]);
G_M = 1000.*diag([0,0,1.0284,0.1622,0.1622,0]);

% Scaling laws from Model scale to Full Scale
MRB(1:3,:) = rho_F/rho_M*(lambda^3).*MRB_M(1:3,:);
MRB(4:6,:) = rho_F/rho_M*(lambda^4).*MRB_M(4:6,:);
MA(1:3,:) = rho_F/rho_M*(lambda^3).*MA_M(1:3,:);
MA(4:6,:) = rho_F/rho_M*(lambda^4).*MA_M(4:6,:);
Minv = inv(MRB + MA);
D(1:3,:) = rho_F/rho_M*(lambda^(2.5)).*D_M(1:3,:);
```

```
D(4:6,:) = rho_F/rho_M*(lambda^(3.5)).*D_M(4:6,:);
G(1:3,:) = rho_F/rho_M*(lambda^2).*G_M(1:3,:);
G(4:6,:) = rho_F/rho_M*(lambda^3).*G_M(4:6,:);

%% Thruster system
alpha_thr = [0,pi/2,pi/2,pi,pi,-pi/2,-pi/2,0]; % Thruster angles
R_thr = [57,52,-52,-57,-57,-52,52,57
         40,45,45,40,-40,-45,-45,-40
         -23,-23,-23,-23,-23,-23,-23,-23]; % Thruster positions
nr = 8; % Number of thrusters
K = eye(nr); % Thruster gain matrix
Kinv = inv(K); % invers of K
T = zeros(6,nr); % Thruster allocation matrix
t = zeros(6,1); % Allocation vector for each thruster
for i=1:nr
    t = [cos(alpha_thr(i))
         sin(alpha_thr(i))
         0
         - R_thr(3,i)*sin(alpha_thr(i))
         R_thr(3,i)*cos(alpha_thr(i))
         R_thr(1,i)*sin(alpha_thr(i))- R_thr(2,i)*cos(alpha_thr(i))];
     T(:,i) = t;
end
Tpinv = pinv(T); % Inverse of T

%% Environmental forces

% Irregular wave model
start = 0.04;
Delta = 0.05;
stop = 4;
L = ceil((stop-start)/Delta);
omega_rand = zeros(1,L);
phase_rand = zeros(1,L);
F_wave = zeros(1,L);
A_wave = zeros(1,L);
i = 1;
for w = start:Delta:stop
    omega_rand(i) = w + Delta*(rand()-0.5);
    phase_rand(i) = 2*pi*rand();
    i = i+1;
end
omega = omega_rand;
T1 = 2*pi/0.8;
Hs = 1;
gamma = 3.3;
F_bar = 0.1;
for i = 1:length(omega)
    w = omega_rand(i);
    if w(1,1) <= 5.24/T1
        sigma = 0.07;
    else
```

```
        sigma = 0.09;
    end
    Y = exp(-((0.191*w(1,1)*T1-1)/(sqrt(2)*sigma))^2);
    S = 155.*Hs^2/(T1^4*w(1,1)^5)*exp(-944/(T1^4*w(1,1)^4))*gamma^Y;
    A_wave(i) = 2*S*Delta;
    F_wave(i) = 1025*9.81*F_bar*A(i);
end

% Current
tau_current = zeros(1,6); % Zero current

%% Mooring system 6DOF
Gm = 10^4.*diag([0.035,0.038,0,0,0,210]); % Linear stiffness mooring matrix
Dm = diag([0,0,0,0,0,0]);% Linear damping mooring matrix

%% Mooring system
% Positions of top points on the rig
R_tp = [59,-59,-59,59
    47.5,47.5,-47.5,-47.5];
% Initialization
cable_param
depth = 200;
R_moor = 300; % Radius of anchor configuration
L_moor = 300; % Mooring cable unstretched lengths
N_moor = 4; % Number of mooring lines
cable_pos
alpha_0 = pi/180.*[45,135,-135,-45]; % Initial mooring cable angles

%% Reference model
% Tuning parameters
zeta_r = [0.1,0.1,0.1];
omega_r = [0.02,0.02,0.02];
t_r = [100,100,100];
% Reference model matrices
Omega = 2.*diag([zeta_r(1)*omega_r(1),zeta_r(2)*omega_r(2),zeta_r(3)*omega_r(3)]);
Gamma = diag([omega_r(1)^2,omega_r(2)^2,omega_r(3)^2]);
A_f = diag([1/t_r(1),1/t_r(2),1/t_r(3)]);

%% Controller gains
% Roll-pitch damping controller
Grpd = (-1)*(10^7).*[0,1;1,0;0.01,0];

% PID regulator gain matrices
Kp = 10^5.*diag([1,1,1000]);
Ki = 10^1.*diag([1,1,100]);
Kd = 10^7.*diag([1,1,1000]);

%% Nonlinear Passive Observer
npo

%% RUN
% Run mooring system
```

```
sim CyberrigI
% Plot Data
plotting
```

Appendix E

Proposed Improvements for CyberRig I

The model semi-submersible CyberRig I is not easily managable in its present state. During model test set-up and execution, the model rig offered several challenges:

- The 'wells' containing the thruster step motors are not watertight and can accidentally be filled with water. The stability of the rig might then be fatally reduced and the step motors put out of action.
- The rig has a moonpool in the center, open only from below the platform deck.
- The yellow coating is old and easily cracked, that means, the rig can not withstand rough treatment or encounter sharp objects.
- The added column cross-sections are not covered with waterproof coating, and tend to absorb significant amounts of water while submerged.
- The model rig can only be tested for stationkeeping control systems due to the need for cabled power supply and ethernet connection, i.e. CyberRig I is not wireless.
- The only computer compatible with the equipment installed on CyberRig I is about 7 years old. The same is true for the software used. The software installed is not longer in use for any other models in the MCLab.

Extensive challenges inspires creative solutions:

- The wells can be covered using some plastic material, e.g. from plastic bags, to avoid water dripping from above.
- Limiting the wave height for model tests can prevent flooding of the moonpool.

- The power and ethernet cables were attached to crannies in the roof to avoid cable-to-water contact and prevent the cables from imposing horizontal forces on the semi-submersible. For the moored configuration, this proved a good solution.

On the other hand, some problems are not easily dealt with. The problem with easily cracked coating is one of them. An extensive treatment with a plastic-type coating for the hole submerged part of CyberRig I is suggested.

An other type of software is now being installed on all model vessel in the MCLab, except for CyberRig I. The upgrading is done for several reasons. A simultaneous hardware and software update for Cyberrig I should be considered.

As suggested in Chapter 5, a gyroscope might well be installed and implemented for CyberRig I. Else, angular velocity estimates for the RPD controller will hardly be obtained.

Several of the mentioned problems can be dealt with in the short run. The problems with the coating, on the other hand, should be assessed imeditately if CyberRig is intended for use in future experiments.

Appendix F

Attachments

In addition to the written Master's Thesis, a zip-file is submitted. The zip-file contains the following elements:

- Master exhibition poster (required for students submitting a Master's Thesis at the Department of Marine Technology, NTNU).